Ore Geology Reviews 99 (2018) 166–179

Contents lists available at ScienceDirect

Ore Geology Reviews

journal homepage: www.elsevier.com/locate/oregeorev

In-situ LA-ICP-MS trace element analyses of scheelite and wolframite: Constraints on the genesis of veinlet-disseminated and vein-type tungsten deposits, South China

Qiang Zhang[a], Rong-Qing Zhang[a], Jian-Feng Gao[b], Jian-Jun Lu[a,*], Jin-Wei Wu[a]

[a] State Key Laboratory for Mineral Deposits Research, School of Earth Sciences and Engineering, Nanjing University, Nanjing 210023, China
[b] State Key Laboratory of Ore Deposit Geochemistry, Institute of Geochemistry, Chinese Academy of Sciences, Guiyang 550081, China

ARTICLE INFO

Keywords:
Veinlet-disseminated scheelite
Vein-type wolframite
LA-ICP-MS analyses
Mineralization process
South China

ABSTRACT

Veinlet-disseminated and vein-type tungsten deposits are important tungsten resources in South China and show remarkable diversity in dominant tungsten minerals. To better understand their genesis, scheelite from the Shimensi veinlet-disseminated deposit and wolframite from the Xihuashan and Piaotang vein-type deposits were selected to conduct in-situ laser ablation-inductively coupled plasma-mass spectrometry trace element analyses.

The Shimensi tungsten mineralization occurs in intensively altered granitic rocks and is characterized by scheelite. Two generations of scheelite in a single grain can be identified by cathodoluminescence (CL) imaging. The early scheelite (dark domains in CL images) is characterized by nearly flat chondrite-normalized REE (REE_N) patterns with significantly negative Eu anomalies, whereas the late one (bright domains in CL images) shows light rare earth element (LREE)-enriched REE_N patterns and obviously positive Eu anomalies. The former has higher REE, Na, Nb and Ta and lower Sr contents than the latter. The Xihuashan and Piaotang wolframite-quartz veins are developed in greisenized granite (type I) and metasedimentary rocks (type II). Both types of wolframite show LREE-depleted patterns, but type I exhibits strongly negative Eu anomalies and type II positive Eu anomalies. Type I contains higher REE, Nb and Ta concentrations, and lower FeO/MnO ratios than type II.

Variations of Eu anomalies and trace element compositions in both scheelite and wolframite can be used to decipher the origin and processes of tungsten mineralization. Both the early scheelite and wolframite (type I) display significantly negative Eu anomalies and have high REE, Nb and Ta contents, suggesting that the initial ore-forming fluids were of magmatic origin. Precipitation of tungsten minerals and alteration would effectively modify the composition of ore-forming fluids. Deposition of the early tungsten minerals would lower REE, Nb and Ta in the mineralizing fluids, leading to depletion of these elements in the late ones. Although both the type I and II wolframite have different REE contents and Eu anomalies, they show similar left-dipped REE_N patterns, implying that compositional variation of fluids is likely driven by crystallization of wolframite during the processes of fluid evolution. In contrast, the elevated LREE/HREE (heavy rare earth element) ratios, δEu (Eu_N/Eu_N^*) values and Sr abundances in the late scheelite are possibly caused by the decomposition of plagioclase and K-feldspar. Alteration plays an important role in the formation of veinlet-disseminated scheelite deposits. It can be concluded that vein-type wolframite mineralization is mainly formed by filling and that veinlet-disseminated scheelite mineralization is associated with metasomatism.

1. Introduction

Veinlet-disseminated scheelite and vein-type wolframite deposits are two important types of tungsten deposits in South China. These two tungsten mineralization types differ in alteration intensity and scale, mineral association, country rock compositions and vein systems, indicating different mechanisms for ore formation. Veinlet-disseminated scheelite deposits are hosted in granitic rocks and associated with pervasive alteration (Xiang et al., 2013). Ore minerals are dominated by scheelite, which occurs in veinlets or is disseminated in altered granitic rocks (Jiang et al., 2015; Sun and Chen, 2017; Xiang et al., 2013). Vein-type wolframite deposits are hosted within both strata and granitic rocks (Sheng et al., 2015; Zhao et al., 2017). Alteration is well developed in granites but very weak in strata (Chen et al., 2008). Wolframite as the main ore mineral occurs mainly in large veins within strata but sometimes dominantly within granitic rocks (Lecumberri-Sanchez et al.,

* Corresponding author.
E-mail address: lujj@nju.edu.cn (J.-J. Lu).

https://doi.org/10.1016/j.oregeorev.2018.06.004
Received 30 December 2017; Received in revised form 22 May 2018; Accepted 1 June 2018
Available online 08 June 2018

2017). Although previous studies have proposed numerous precipitation mechanisms, the origin of these two mineralization types remains debated. For vein-type wolframite deposits, phase separation (Korges et al., 2018), fluid mixing (Vallance et al., 2001; Wei et al., 2012) and fluid-rock interaction (Codeço et al., 2017; Lecumberri-Sanchez et al., 2017) have been identified as possible mechanisms for wolframite precipitation. However, only fluid-rock interaction is considered to have played an important role in the formation of veinlet-disseminated scheelite deposits (Sun and Chen, 2017). Thus, further research is needed to determine whether differences in fluid evolution processes control what type of tungsten deposits forms.

Recently, in-situ analyses of minerals are widely used in tracing detailed mineralization processes (Crowe et al., 2001; Huang et al., 2015; Reich et al., 2013; Zhao and Zhou, 2015; Zhu et al., 2015). Scheelite and wolframite are the dominant tungsten minerals in veinlet-disseminated and vein-type tungsten deposits, respectively. Both of them can incorporate significant amounts of REE, Nb, Ta and other trace elements (Goldmann et al., 2013; Guo et al., 2016; Sun and Chen, 2017; Xiong et al., 2017). Extensive studies demonstrated that the contents of trace elements and their variations in scheelite and wolframite can record the physicochemical conditions and compositions of ore-forming fluids, and thus reflect their source and evolution. Zhao et al. (2018) showed that the behavior of the REE in scheelite could be used to quantitatively reconstruct the changing physicochemical conditions during ore formation. Song et al. (2014) documented that high Mo scheelite in skarn-type W-Mo deposits formed under oxidized condition. Ghaderi et al. (1999) addressed that two types of scheelite from the Archean hydrothermal gold deposits in Western Australia precipitated from oxidized Na-rich and reduced Na-poor fluids, respectively. Brugger et al. (2000) demonstrated that heterogeneous composition of scheelite was caused by the evolution of hydrothermal fluids. Sun and Chen (2017) argued that the evolution of ore-forming fluids at the giant Dahutang deposit, inferred from trace element compositions of scheelite, resulted from fluid-rock interaction. Harlaux et al. (2018) considered that ore-forming fluids and metals in hydrothermal W deposits from the French Massif Central were mainly sourced from evolved peraluminous granites on the basis of chemical compositions of wolframite. However, few studies have compared the compositional evolution of fluids and the controlling factors for different types of tungsten deposits, which hinders our better understanding of tungsten mineralization systems.

The Dahutang deposit, located in northwestern Jiangxi Province, is a giant tungsten deposit with estimated reserves of 2 million tons of WO_3 and is characterized by veinlet-disseminated scheelite mineralization in granitic rocks (Mao et al., 2013b). The Xihuashan and Piaotang deposits in southern Jiangxi Province are two large-scale vein-type wolframite deposits, and contain reserves of 121,000 t and 92,000 tons of WO_3, respectively (Mao et al., 2013a). Wolframite-quartz veins in Xihuashan are mainly hosted in granite, and those in Piaotang dominantly in metasedimentary rocks. These three deposits provide a good opportunity for comparing the genesis of the two types of tungsten mineralization. In this paper, we performed in-situ LA-ICP-MS trace element analyses of scheelite from the Shimensi ore section in the Dahutang deposit and wolframite from the Xihuashan and Piaotang deposits. By using the trace element datasets of these tungsten minerals, this paper constrained the source and evolution of ore-forming fluids and revealed different ore-forming processes of these two tungsten deposits types.

2. Geological background

The South China Block is composed of the Yangtze Block to the northwest and the Cathaysia Block to the southeast, and contains two important tungsten deposit belts, i.e. the E-W-trending Nanling Range metallogenic belt and the Jiangnan Orogen (Fig. 1). Exposed strata in the Nanling Range comprise weakly metamorphosed Precambrian-Ordovician flysch-volcanic sequences, folded Late Devonian-Early Triassic shallow marine carbonate-argillaceous-arenaceous sequences and Late Triassic-Paleocene terrigenous clastic-volcanic rock formation (Shu et al., 2006). Granites formed during the Late Ordovician-Silurian, Triassic and Jurassic-Cretaceous in this region (Chen et al., 2013; Shu et al., 2006). It is now generally accepted that tungsten deposits are genetically related to these granites, especially the Late Jurassic granites (Chen et al., 2008, 2013; Mao et al., 2013a, 2007; Zhao et al., 2017).

The Jiangnan Orogen was formed by amalgamation of the Yangtze and Cathaysia Blocks during the Neoproterozoic (Li et al., 2009; Wang et al., 2007, 2014) and is characterized by widespread occurrence of Neoproterozoic greenschist-facies metamorphosed sedimentary rocks. In addition to the Paleozoic and Mesozoic granites, the Neoproterozoic granitic rocks such as the Jiuling batholith in northern Jiangxi Province are widely distributed within this orogen. The super-large Dahutang and Zhuxi tungsten deposits have been discovered in this area and are considered to be related to the Mesozoic granites (Huang and Jiang, 2014; Mao et al., 2013b, 2015; Zhao et al., 2017).

3. Deposit geology

3.1. The Dahutang deposit

The Neoproterozoic Shuangqiaoshan Group, a suite of thick greenschist-facies volcanic-clastic sedimentary rocks, is present in the Dahutang deposit (Fig. 2a). Fault structures at Dahutang comprise an E-W-trending ductile shear zone, a NNE-striking basement fault, NNE-NE and NNW-NW-striking faults and stockwork fractures (Fig. 2). The former two structures control the emplacement of Mesozoic granites and distribution of the tungsten deposits (Mao et al., 2013b). Wolframite-scheelite quartz veins occur mainly along the NNE-NE and NNW-NW striking faults. The stockwork fractures control the veinlet-disseminated mineralization (Xiang et al., 2012).

Exposed intrusions at Dahutang include the Neoproterozoic biotite granodiorite and Mesozoic granites (Fig. 2). The latter consist mainly of porphyritic and fine-grained biotite granite, two-mica granite, muscovite granite and granite porphyry (Huang and Jiang, 2014; Jiang et al., 2015; Mao et al., 2015). In the Shimensi ore section, the porphyritic biotite granite is cut by the subordinate fine-grained biotite granite (Fig. 2b). The granite porphyry formed later than both the porphyritic and fine-grained biotite granite. A pegmatite shell (0.2–1.5 m thick) occurs at the top of the porphyritic biotite granite. These Mesozoic granites are highly fractionated S-type granites and are considered to be associated with the tungsten mineralization (Huang and Jiang, 2014; Mao et al., 2015).

The Dahutang deposit comprises three ore sections: Shiweidong, Dawutang, and Shimensi (Fig. 2a). The Shimensi ore section is the largest W-Cu-Mo deposit at Dahutang and has reserves of > 740,000 tons of WO_3 with an average grade of 0.195% WO_3 (Xiang et al., 2013). At Shimensi, the mineralization types are dominated by veinlet-disseminated type with subordinate breccia and vein type (Fig. 2b), which contribute to > 90%, 5% and 1% of the total tungsten reserves, respectively (Jiang et al., 2015; Mao et al., 2013b). The veinlet-disseminated mineralization occurs mainly in Neoproterozoic biotite granodiorite and subordinately in Mesozoic granites as thick stratiform-like ore bodies. Ore minerals are mainly scheelite with minor wolframite. Scheelite occurs mainly in quartz veinlets with a width of less than 2 cm (Fig. 3a) and in the surrounding altered rocks. Wall-rock alteration is characterized by pervasive greisenization around veinlets (Fig. 3). The breccia-type mineralization is mainly situated in the apical part of the Mesozoic porphyritic biotite granite, and is marked by the presence of breccia fragments of granodiorite and porphyritic biotite granite that are cemented by ore-bearing quartz. Tungsten minerals in the vein-type mineralization are dominated by wolframite and subordinate scheelite. Quartz veins in this type mineralization commonly

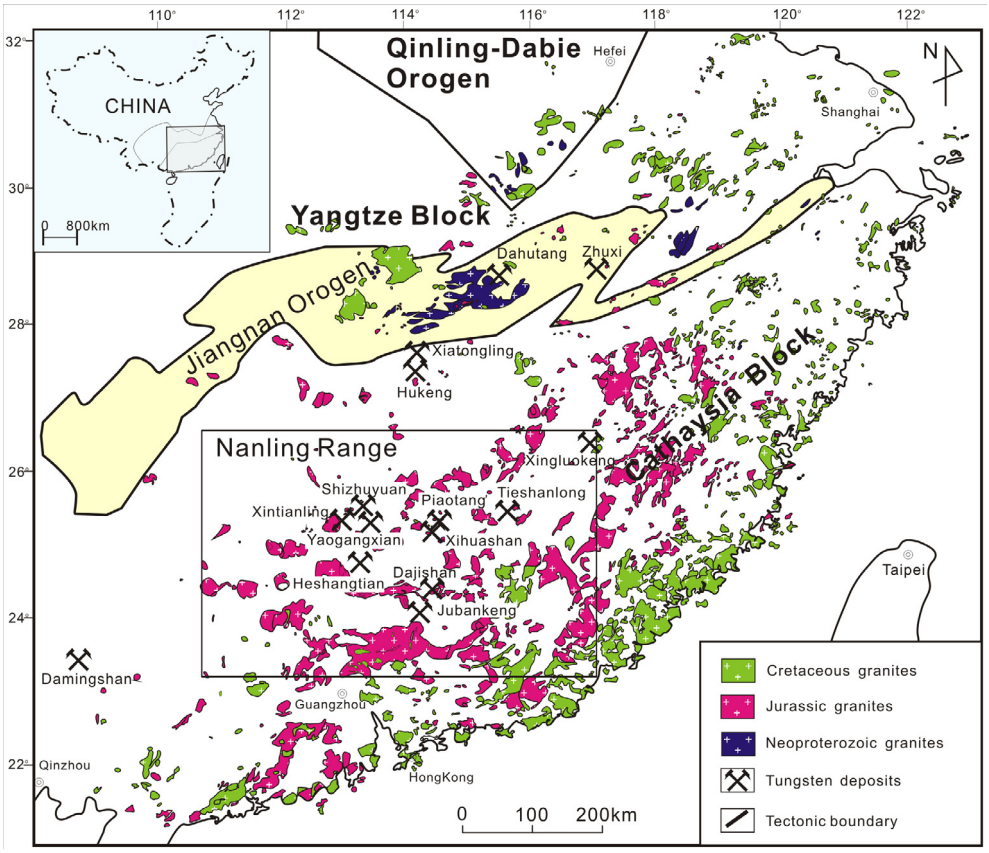

Fig. 1. Distribution of major Mesozoic tungsten deposits in South China (modified after Mao et al., 2013a; Zhou et al., 2006).

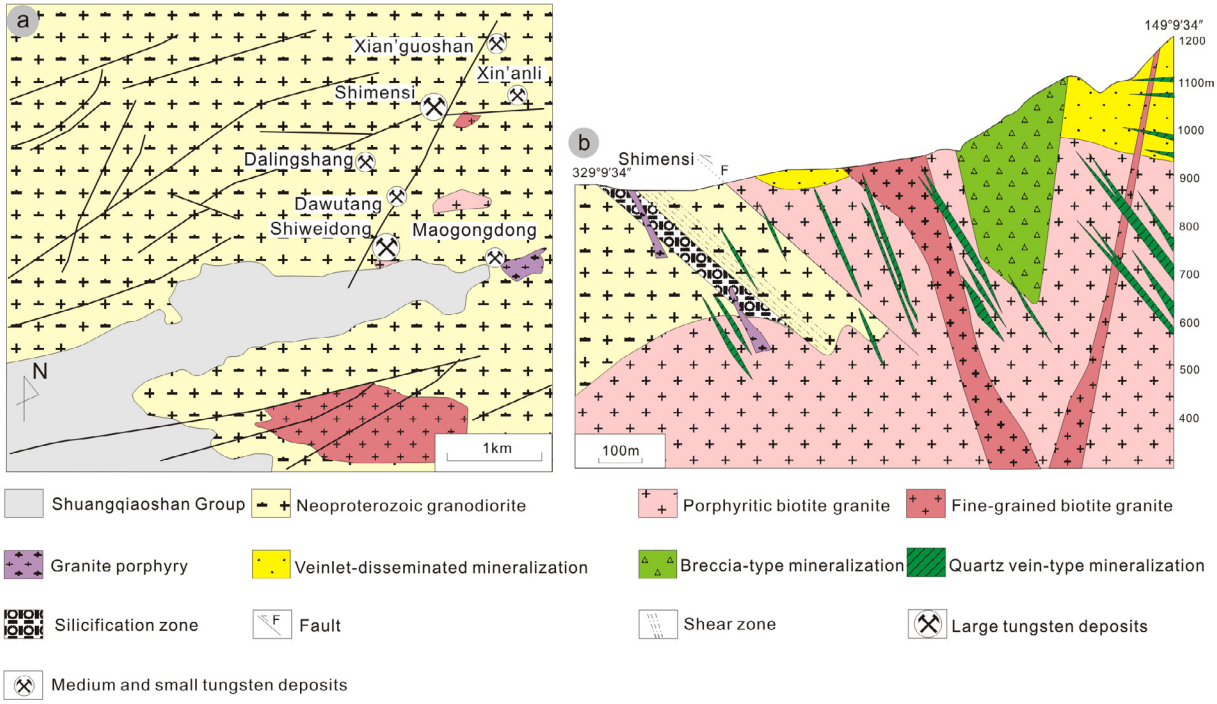

Fig. 2. (a) Simplified geological map of the Dahutang tungsten deposit (modified after Sun and Chen, 2017). (b) Cross section of the Shimensi ore section showing three types of tungsten mineralization: veinlet-disseminated, breccia and quartz-vein type (modified after No. 916 Geological Team, Jiangxi Bureau of Geology, Mineral Resources, Exploration and Development, 2012).

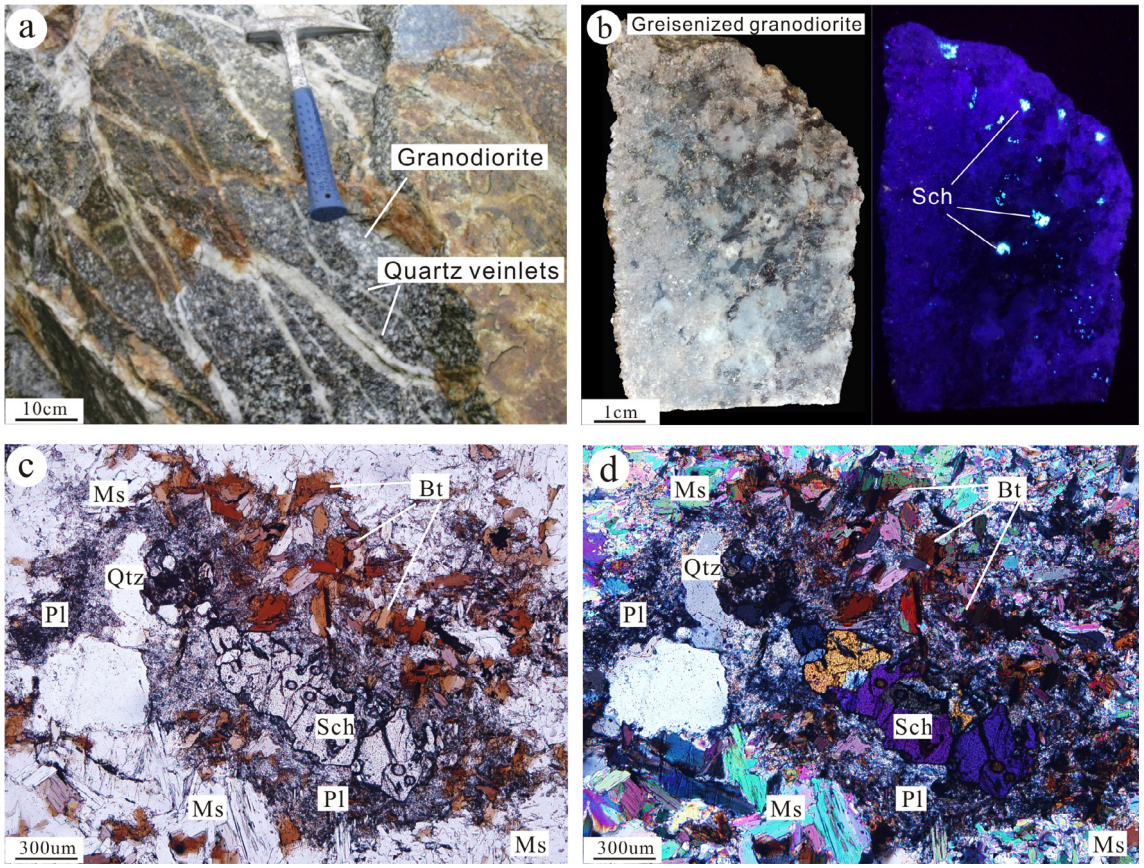

Fig. 3. (a) Veinlet-disseminated mineralization in Neoproterozoic granodiorite in the Shimensi ore section. (b) Disseminated scheelite in greisenized granodiorite in the Shimensi ore section. (c-d) Photomicrographs of disseminated scheelite in greisenized granodiorite (c: transmitted plane-polarized light; d: transmitted cross-polarized light); circles on scheelite represent laser ablation pits. Mineral abbreviations: Bt, biotite; Fl, fluorite; Ms, muscovite; Pl, plagioclase; Qtz, quartz; Sch, scheelite.

have a width of more than 10 cm and are bordered by greisen selvages of several to tens of centimeters in width.

3.2. The Xihuashan and Piaotang deposits

Upper Cambrian low-grade metamorphosed flysch-like sedimentary rocks, including sandstone and slate, are exposed in the Xihuashan and Piaotang deposits (Figs. 4 and 5). The EW-trending faults control the emplacement of granitic intrusions and tungsten mineralization in the deposits.

The Xihuashan granitic complex contains four phases, namely medium-grained, medium- to fine-grained and fine-grained porphyritic biotite granite, and medium-grained biotite granite (Li et al., 1986; Fig. 4). These granites were formed at 158–161 Ma (Guo et al., 2012) and are thought to be highly evolved S-type granites (Lv et al., 2011; Xiao et al., 2009). Tungsten mineralization at Xihuashan is related to both medium-grained biotite granite and medium-grained porphyritic biotite granite (Wang and Zhou, 1982). Xihuashan is a large-scale vein-type tungsten deposit (Figs. 4 and 6a) that contains reserves of 121,000 tons of WO_3 with an ore grade of 0.63–1.06% WO_3 (Mao et al., 2013a). Ore-bearing quartz veins commonly have thickness of 0.2–0.6 m, occur in clusters and show an echelon distribution. Hydrothermal alterations around veins comprise potassic alteration, greisenization (Fig. 6b), silicification and sericitization, which display horizontal and vertical zonation (Liu, 1989). Based on mineral assemblages and crosscutting relationships, ore-forming processes include an early silicate-oxide stage, a sulfide stage and finally a carbonate stage (Giuliani et al., 1988; Wei et al., 2012). The silicate-oxide stage formed massive quartz, wolframite, molybdenite, cassiterite, beryl and feldspar. The sulfide stage is featured by assemblages of pyrite, arsenopyrite, chalcopyrite, sphalerite and galena with minor wolframite. The carbonate stage generated calcite and quartz with trace amounts of chalcopyrite and pyrite but no wolframite.

Intrusive rocks at Piaotang include exposed quartz diorite and hidden stock-like granite (Fig. 5), which were emplaced at 434–439 Ma and 158–160 Ma, respectively (He et al., 2010; Li et al., 2010; Zhang et al., 2017). Three facies exist in the granite from bottom to top, i.e. porphyritic biotite granite, two-mica granite and muscovite granite (Zhang et al., 2017). This granite is classified as a highly fractionated S-type (Zhang, 2004) and is closely associated with the tungsten mineralization (Zhang et al., 2017). The Piaotang tungsten deposit contains total metal reserves of 92,000 tons of WO_3 (0.154% WO_3 ore grade) and 64,000 tons of Sn (0.115% Sn ore grade) (Mao et al., 2013a). Veins system at Piaotang shows a five-floor vertical zonation from cupola of granite to metasedimentary rocks, namely: pinch-out zone, large vein zone (Fig. 6c), thin vein zone, veinlet/stockwork zone (Fig. 6d) and stringer zone (Gu, 1979, 1984). The veinlet/stockwork zone and thin vein zone in the metasedimentary rocks host 72% of the total tungsten reserves in this deposit (Zhang et al., 2017). Around the veins, strong potassic alteration and greisenization occur in granite (Fig. 6e) and weak muscovite alteration halos in the metasedimentary rocks (Fig. 6f). Based on crosscutting relationships and mineral associations, seven mineralizing stages have been recognized (Li et al., 1993): garnet-diopside skarn (stage I), molybdenite-(wolframite)-quartz veins (stage II), cassiterite-wolframite-quartz veins (stage III), wolframite-cassiterite-sulfide-quartz veins/veinlets (stage IV), sulfide-quartz veins (stage V), chlorite-quartz veins (stage VI) and fluorite-calcite veins (stage VII). Stage II, III and IV are the main tungsten mineralizing stages

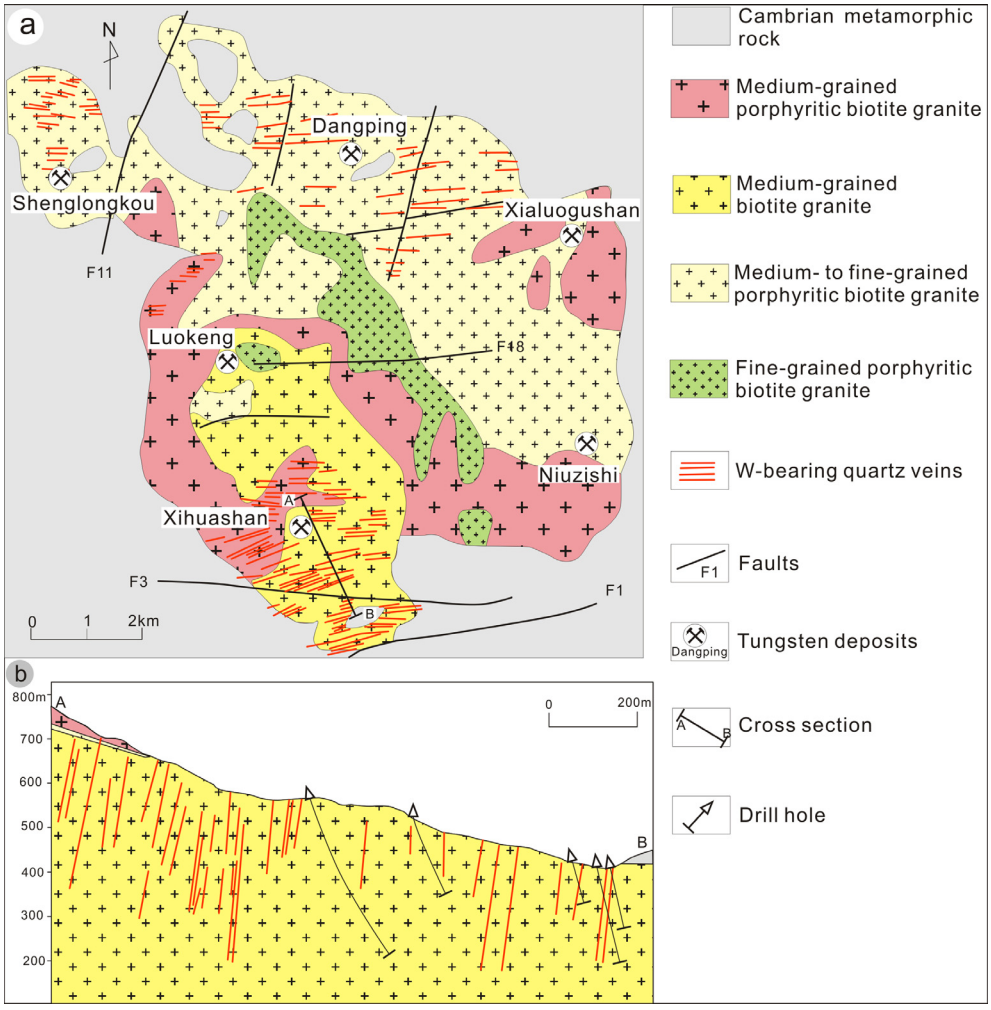

Fig. 4. (a) Geological map of the Xihuashan tungsten deposit (modified after Li et al., 1986; Wang et al., 2003). (b) Cross section of tungsten orebodies (modified after Hu et al., 2012).

and contribute 13%, 17% and 64% of the total tungsten reserves, respectively (Zhang et al., 2017).

4. Sampling and analytical methods

4.1. Scheelite and wolframite samples

Disseminated scheelite in the altered Neoproterozoic granodiorite from the Shimensi ore section was sampled. Wolframite sample 16XHS01b-2 from Xihuashan was taken from the quartz-wolframite-molybdenite vein in the medium-grained biotite granite at 100 m level. Wolframite samples 16PT10a and 16PT03c1 from Piaotang were collected from the quartz-wolframite-cassiterite vein (stage III) in the granite at 268 m level and from the quartz-wolframite-cassiterite-sulfide vein (stage IV) in the metasedimentary rocks at 556 m level, respectively. These samples were prepared as polished probe sections for in-situ laser ablation-inductively coupled plasma-mass spectrometry (LA-ICP-MS) analyses.

4.2. LA-ICP-MS

LA-ICP-MS analysis was performed at the FocuMS Technology Co. Ltd., Nanjing, China. Laser sampling was performed using a Cetac Photon Machines 193 nm ArF excimer laser ablation system, coupled to an Agilent 7700x ICP-MS. A 40um spot was used with an energy density of 5.6 J/cm^2 and a repetition rate of 5 Hz. Each LA-ICP-MS analysis incorporated a ~15 s background acquisition (gas blank) and a 40 s data acquisition from the sample. Every nine-spot analysis was followed by one NIST SRM 610 analysis to correct the time-dependent drift of sensitivity and mass discrimination of the ICP-MS. Reference glasses (NIST612, NIST610) were analyzed prior to and after the sample measurements. The NIST SRM 610 was used as the external standard and data reduction was performed using the ICPMSDataCal software (Liu et al., 2008).

5. Results

5.1. Internal textures of scheelite and wolframite

Scheelite from Shimensi shows complex zoning of dark and bright domains in cathodoluminescence (CL) images. Two generations of scheelite exist and the early generation (dark domains in CL image) is replaced and cemented by the late generation (bright ones) (Fig. 7).

Wolframite hosted in the granite has zones consisting of regular succession of micrometer-sized growth bands (Fig. 8a and b) and one in the metasedimentary rocks shows homogeneous internal textures under transmitted infrared radiation (IR) (Fig. 8c).

5.2. Trace element geochemistry of wolframite from Xihuashan and Piaotang

Major and trace element compositions of wolframite in Xihuashan

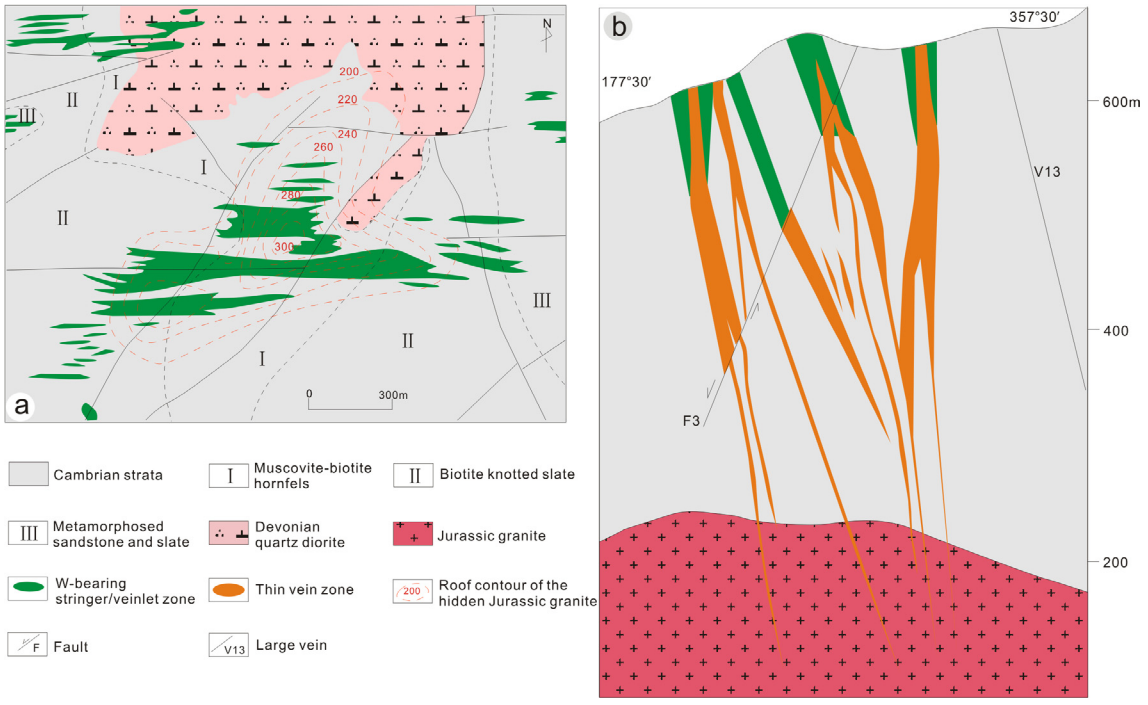

Fig. 5. (a) Geological map of the Piaotang tungsten deposit (modified after Shan, 1976). (b) Cross section of tungsten orebodies along the No. 12 exploration line (modified after No. 2 Team of Jiangxi Metallurgical Geology, 1978).

and Piaotang are showed in Table 1. Although all of the wolframite samples display similar chondrite-normalized REE (REE_N) patterns (heavy rare earth element (HREE)-enriched), wolframite hosted within the granite (type I) at Xihuashan and Piaotang has compositions different from that in the metasedimentary rocks (type II) at Piaotang (Fig. 9). Type I wolframite has significantly negative Eu anomalies, whereas type II shows positive Eu anomalies. In addition, type I has lower FeO/MnO ratios and higher REE, Nb and Ta contents than type II (Table 1; Fig. 9b).

5.3. Trace element geochemistry of scheelite from Shimensi

Analytical results of scheelite at Shimensi are given in Table 2. REE_N patterns and trace element diagrams for scheelite are presented in Fig. 10. Two generations of scheelite have distinct REE_N patterns and trace element compositions. The early generation is characterized by nearly flat REE_N patterns with significantly negative Eu anomalies, while the late one is of light rare earth element (LREE)-enriched REE_N patterns and obviously positive Eu anomalies. The former has higher REE, Na, Nb and Ta, and lower Sr concentrations than the latter (Fig. 10).

6. Discussion

6.1. Source and evolution of ore-forming fluids for vein-type mineralization

Wolframite and quartz from quartz veins within the granite in Xihuashan have $\delta^{18}O$ values from 4.92 to 6.94‰ and 11.98 to 13.95‰, respectively, corresponding to the $\delta^{18}O$ values of ore-forming fluids of 6.33 to 8.27‰ (Mu et al., 1982). The ranges of $\delta^{18}O$ values of wolframite (3.67–7.61%) and quartz (11.47–13.62‰) from Piaotang are similar to those in Xihuashan, yielding $\delta^{18}O_{H2O}$ values of 4.90–8.86‰ (Mu et al., 1982). The oxygen isotopic compositions of these fluids forming ore-bearing veins suggest a magmatic origin.

Compared to LREE, the ionic radii of HREE (Gd^{3+}-Lu^{3+}: 0.94–0.86 Å) are much closer to those of Fe^{2+} (0.78 Å) and Mn^{2+} (0.83 Å) in octahedral site (Shannon, 1976), and hence HREE have higher wolframite-fluid partition coefficients than LREE. This explains the LREE-depleted REE_N patterns exhibited by type I and type II wolframite, which differ from the host granite (Fig. 9a). Due to the lack of the partition coefficient for each element in wolframite, REE_N patterns of wolframite cannot be used to trace the source of mineralizing fluids directly. Although type I wolframite from the granite in Xihuashan and Piaotang has different REE concentrations, it has significantly negative Eu anomalies, similar to the host granite (Fig. 9a). Wolframite grains from the medium- to low-temperature Woxi Au-Sb-W deposit, with no evidence showing its genetic relation to granite by far, have low Nb-Ta contents (< 2 ppm) and no clear Eu anomalies (Zhu et al., 2014). However, wolframite samples in quartz vein systems, which are genetically correlated with highly evolved and Eu-depleted granite, exhibit strongly negative Eu anomalies and elevated Nb-Ta contents (Harlaux et al., 2018; Zhang et al., 1990; Zhang, 2012). Thus, such negative Eu anomalies of the wolframite in the two deposits are likely inherited from the highly fractionated host granite. Nb and Ta are commonly concentrated in high temperature fluids, and decrease with decline of temperature (Liu and Cao, 1987). Harlaux et al. (2018) considered that progressive increase of Nb and Ta in wolframite with depth indicated that ore-forming fluids and metals were from hidden granite. Nb and Ta concentrations in wolframite from Piaotang increase from type II (shallow) to type I (deep; Fig. 9b) and type I contains significantly high Nb and Ta (Nb, 2,740–11,000 ppm; Ta, 64.7–7,900 ppm; Table 1), possibly implying that type I has precipitated from high temperature magma-derived fluids.

Type II wolframite contains lower REE (31.5–99.4 ppm, Table 1), Nb (20.9–723 ppm) and Ta (0.19–12.8 ppm) but higher δEu (Eu_N/Eu_N^* = 0.93–2.69) and FeO/MnO (1.8–2.5) values than type I (Fig. 9). Despite the differences in REE contents and Eu anomalies, both types have similar LREE-depleted REE_N patterns, suggesting that fluids forming type II wolframite might have evolved from the fluids that crystallized type I. Brugger et al. (2000) proposed that the precipitation of tungsten minerals could effectively alter the compositions of fluids. Crystallization of type I wolframite with high REE, Nb and Ta would significantly lower these elements in the fluids. Therefore, type II precipitating from evolved fluids would contain relatively lower

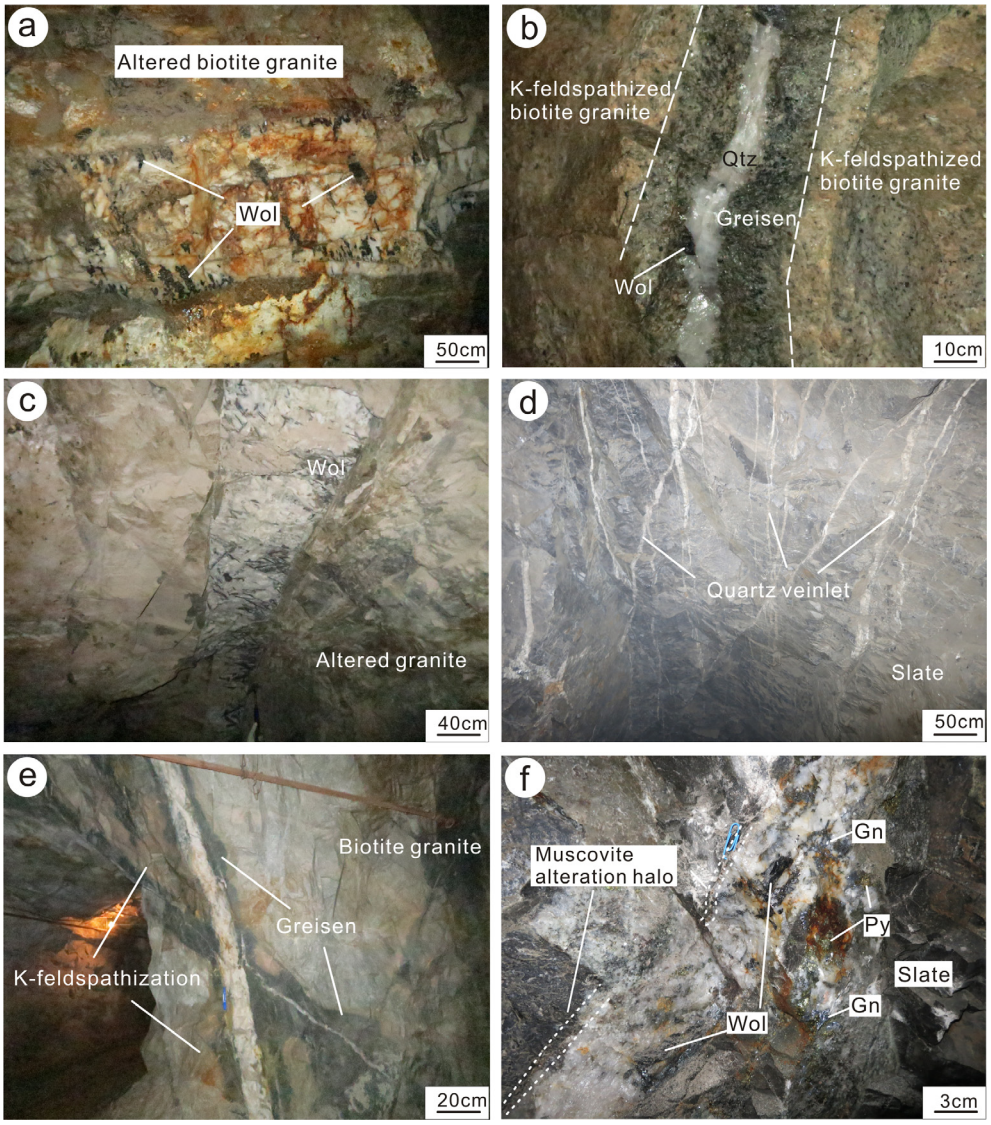

Fig. 6. Mineralization and alteration characteristics of the Xihuashan (a and b) and Piaotang (c–f) deposits. (a) Wolframite-bearing quartz vein hosted in biotite granite at 100 m level. (b) K-feldspathization and greisenization in the sidewalls of quartz vein in granite. (c) Wolframite-bearing quartz vein hosted in granite at 268 m level. (d) Wolframite-bearing quartz veinlets hosted in slate at 556 m level. (e) Greisenization and K-feldspathization around quartz vein in biotite granite at 268 m level. (f) Quartz-wolframite-cassiterite-sulfide veinlet in slate at 556 m level; muscovite alteration halos in the sidewalls of quartz vein. Mineral abbreviations: Gn, galena; Py, pyrite; Qtz, quartz; Wol, wolframite.

concentrations of these elements. Oxygen isotopic compositions of wolframite and quartz from Piaotang indicate that meteoric water was added into vein systems in the metasedimentary rocks (Zhang, 1988). The addition of meteoric water would increase the oxygen fugacity of hydrothermal systems, resulting in elevated Eu^{3+}/Eu^{2+} in fluids. Compared with Eu^{2+} (1.17 Å), the ionic radius of Eu^{3+} (0.95 Å) is much closer to those of Fe^{2+} (0.78 Å) and Mn^{2+} (0.83 Å) (Shannon, 1976) so that partition coefficient of Eu^{3+} between wolframite and fluids is much higher than that of Eu^{2+}. Thus, wolframite-fluid partition coefficient of Eu would increase in the evolved fluids, which might lead to elevated δEu values and weakly positive Eu anomalies in type II wolframite.

6.2. Source and evolution of ore-forming fluids for veinlet-disseminated type mineralization

The source and evolution of ore-forming fluids can be reflected by compositional variations of scheelite (Sun and Chen, 2017; Zhao et al., 2018). In the present study, the early generation of scheelite has higher REE, Nb and Ta and lower Sr concentrations than the late generation (Fig. 10), indicating that the early fluids likely contain high REE, Nb and Ta and low Sr contents.

Significantly negative Eu anomalies of the early generation of scheelite might have been inherited from the highly fractionated granite which also shows negative Eu anomalies (Fig. 10a). High Nb and Ta in the early fluids also indicate a close genetic relationship with the granite (Sun and Chen, 2017). These features suggest a magmatic source for the ore-forming fluids in Shimensi, which is supported by $\delta^{18}O_{H2O}$ values (4.5–7.3‰) of fluid inclusions in quartz from the scheelite-bearing quartz veins (Wang et al., 2015).

Compared to the early generation of scheelite, the late one has lower REE, Nb and Ta concentrations, but higher LREE/HREE ratios (5.86–26.6, Table 2), δEu values (1.09–2.84) and Sr contents (307–423 ppm) (Fig. 10). The decrease of REE, Nb and Ta in the late scheelite is likely caused by precipitation of the early one and the resulting decline of these elements in fluids. It is noteworthy that the late scheelite is highly LREE-enriched, very similar to the porphyritic biotite granite, but different from the early one. Obviously, crystallization of the early scheelite which shows nearly flat REE_N patterns could not result in fractionation of LREE and HREE in fluids and thus the enrichment of LREE in the late one. In addition, the obviously positive Eu anomalies in the late scheelite could not be generated only by precipitation of the early one with negative Eu anomalies. Thus, additional LREE and Eu inputs are required for the evolved fluids to achieve this transition. Tungsten mineralization at Shimensi is closely associated with pervasive greisenization around veinlets in granitic rocks (Fig. 3). Plagioclase and K-feldspar in these rocks would be decomposed during greisenization (Heinrich, 1990). Both plagioclase and K-feldspar are

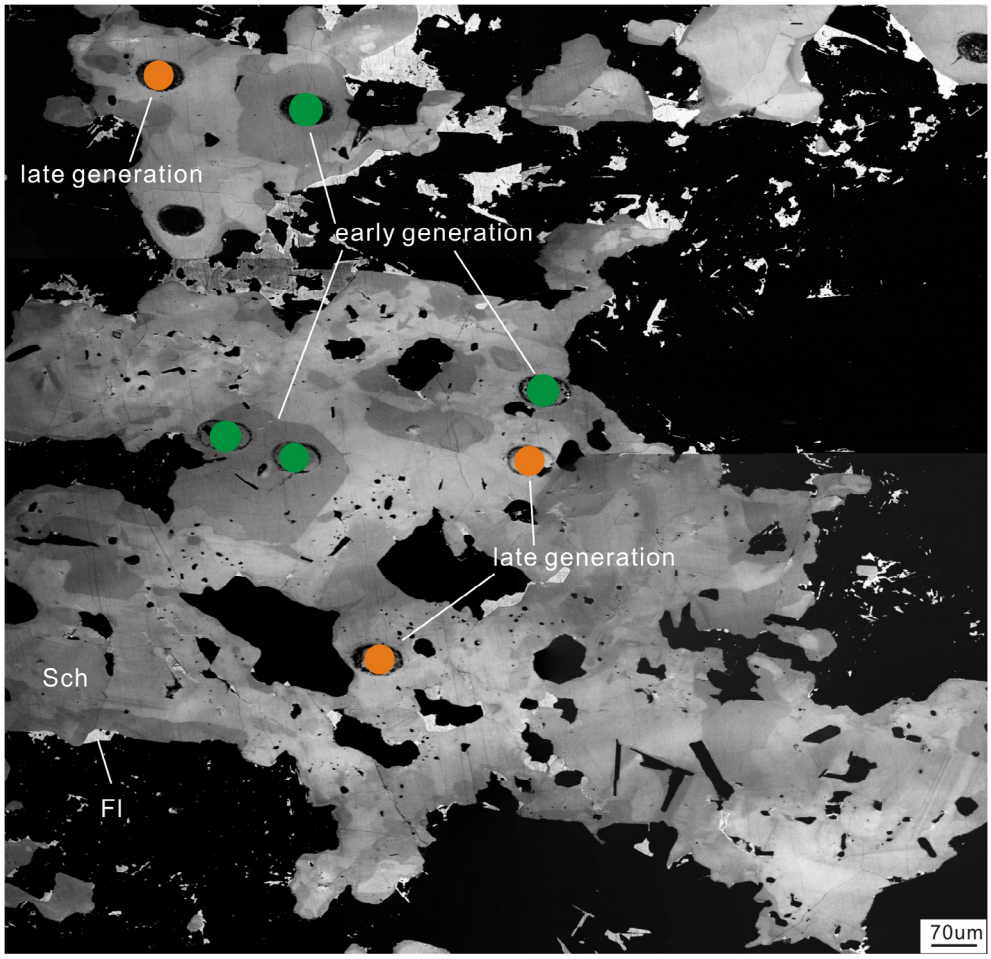

Fig. 7. Representative CL image of scheelite in the Shimensi ore section. Scheelite showing complex zoning texture with dark and bright domains. The circles in CL image represent laser ablation pits. Mineral abbreviations: Fl, fluorite; Sch, scheelite.

characterized by positive Eu anomalies and enrichment of LREE (Arth, 1976), meaning that their decomposition would release LREE and Eu into fluids. Therefore, the scheelite precipitating from such evolved fluids would exhibit obviously positive Eu anomalies and LREE-enriched REE_N patterns.

Sr can substitute for Ca in plagioclase so that plagioclase generally contains high Sr concentrations. The Mesozoic porphyritic biotite granite and Neoproterozoic granodiorite are the main host rocks of the Shimensi tungsten deposit and contain abundant plagioclase. Decomposition of such plagioclase could release significant amounts of Sr into fluids. With progressive alteration, increasing amounts of plagioclase in these granitic rocks would be altered to muscovite and quartz (Fig. 3c and d; Heinrich, 1990), resulting in elevated Sr contents in the late fluids. This explains why the late generation of scheelite, which precipitated from evolved fluids, shows high Sr concentrations.

From the above discussion, it could be concluded that in addition to scheelite crystallization, alteration also played an important role in the evolution of ore-forming fluids of veinlet-disseminated tungsten mineralization.

On the (ΣREE + Y-Eu)-Na diagram (Fig. 11), almost all data show a good linear correlation near the 1:1 correlation line, indicative of the Na-REE coupled substitution mechanism. Variation of Na in scheelite could indicate fluctuating Na concentrations in fluids. From early to late generation of scheelite, Na concentrations show a decreasing trend, suggesting that salinity might decrease during the evolution of fluids.

6.3. Genesis of the two deposit types: filling vs. metasomatism

The Shimensi veinlet-disseminated scheelite mineralization and the Xihuashan and Piaotang vein-type wolframite mineralization are both driven by magma-derived fluids. Oxygen isotope compositions of quartz and wolframite in the three deposits suggest a magmatic origin of the ore-forming fluids (Mu et al., 1982; Wang et al., 2015), as do the $\delta^{34}S$ values (−3.4 to +0.6‰) of sulfide minerals (Mu et al., 1982; Wang et al., 2015; Wei et al., 2012). Early tungsten minerals with obviously negative Eu anomalies and high REE, Nb and Ta contents also show a genetic relationship with granite. Moreover, the formation of greisen around W-bearing veins/veinlets in granitic rocks (Figs. 3 and 6) is thought to be associated with magmatic fluids (Štemprok et al., 2005).

Many mechanisms have been proposed to account for the precipitation of ore minerals in W(-Sn) deposits, such as cooling (Heinrich, 1990; O'Reilly et al., 1997), mixing of magmatic and meteoric fluids (Bychkov and Matveeva, 2008; Sushchevskaya and Bychkov, 2009), a pH increase by boiling and/or CO_2 effervescence due to depressurization (Higgins, 1985; Korges et al., 2018) and fluid-rock interaction (Dewaele et al., 2016; Lecumberri-Sanchez et al., 2017; Sun and Chen, 2017). By using the trace element compositions of tungsten minerals from veinlet-disseminated and vein-type tungsten mineralization, together with other evidences such as fluid inclusions and stable isotopes, two contrasting fluid evolution histories for the two types of deposits have been revealed, and we consider that controlling factors that lead to their ore formation are quite different.

Based on the compositions of fluid inclusions and alteration geochemistry, Lecumberri-Sanchez et al. (2017) argued that interaction of

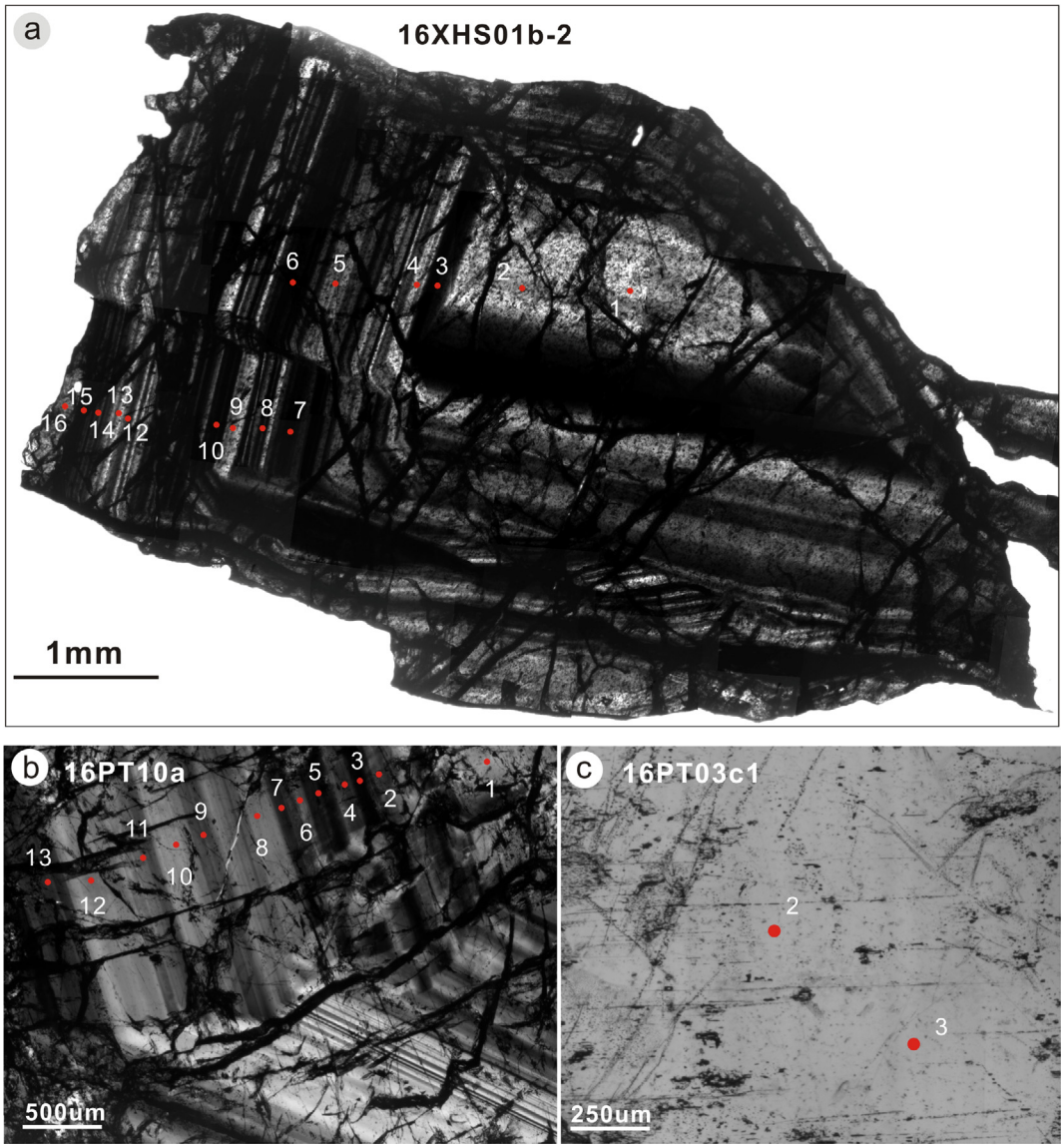

Fig. 8. Representative transmitted infrared images of wolframite in the Xihuashan and Piaotang deposits. Wolframite hosted in the granite from Xihuashan (a) and Piaotang (b) shows growth bands. (c) Wolframite in the metasedimentary rocks from Piaotang displays homogeneous internal texture. Red circles and numbers beside them represent analytical spots by LA-ICP-MS. (For interpretation of the references to colour in this figure legend, the reader is referred to the web version of this article.)

W-rich, Fe-poor magmatic fluids with Fe-rich wall rocks in the Panasqueira (Portugal) vein-type wolframite deposit was the decisive factor for wolframite formation. However, the host granite at Xihuashan and Piaotang is very low in Fe (iron oxide < 1.2%; Guo et al., 2012; Zhang, 2004). Although the metasedimentary rocks at Piaotang contains 4–5% iron oxide and 0.02–0.07% manganese oxide (Li et al., 1986), wall-rock alteration around wolframite-quartz veins in these rocks is extremely weak (Fig. 6d and f). Thus, alteration of these wall rocks unlikely provides sufficient Fe and Mn for fluids to precipitate wolframite. REE, Nb and Ta contents in wolframite show a decreasing trend from type I to II and both types exhibit similar nearly parallel left-dipped REE patterns, implying that compositional evolution of ore-forming fluids is likely mainly controlled by crystallization of wolframite during the formation of quartz vein system by filling and addition of other sources (e.g., wall rocks via fluid-rock interaction) into the evolved fluids might be limited. Thermodynamic modelling indicated that wolframite could be precipitated in large quantities by cooling of an Fe-W-bearing fluid without significant alteration in a confined channel (Heinrich, 1990). Theoretical calculations showed that solubility of tungsten is not only controlled by temperature, but also by salinity and pH, and decreases with decreasing temperature and salinity, and increasing pH (Wood and Samson, 2000). Fluid inclusion studies revealed that fluid depressurization usually occurred during fracture opening in vein systems (Giuliani et al., 1988; Korges et al., 2018), and that the resulting vapor loss (e.g., of CO_2) from fluids by boiling would lead to an increase of pH, which is an effective mechanism for tungsten deposition (Higgins, 1985). Oxygen isotope modelling by wolframite and quartz from Xihuashan implied the mixing of ore-bearing magmatic fluids and meteoric water in ore-forming systems, which may also contribute to wolframite precipitation by dilution and promoting cooling of fluids (Wei et al., 2012). Thus, in the vein-type wolframite deposits, depressurization and phase separation of fluids, and fluid mixing as well as cooling are likely the most effective mechanisms for wolframite deposition.

For the veinlet-disseminated mineralization system at Shimensi, fluid compositions are not only modified by scheelite deposition, but also by wall-rock alteration. Compositional changes of fluids by alteration have been recorded by the late scheelite which has elevated

Table 1
Major (wt% oxide) and trace element (in ppm) analytical results of wolframite by LA-ICP-MS in the Xihuashan and Piaotang deposits.

Spots	Piaotang (16PT03c1)											16PT10a											
	2	3	4	5	6	7	8	9	10	11	Mean (n = 10)	1	2	3	4	5	6	7	8	9	10	11	12
La	0.000	0.000	0.000	0.003	0.000	0.003	0.003	0.000	0.000	0.003	0.001	0.003	0.003	0.000	0.04	0.02	0.000	0.003	0.01	0.000	0.000	0.01	0.003
Ce	0.000	0.01	0.000	0.002	0.01	0.004	0.01	0.01	0.002	0.01	0.005	0.05	0.04	0.05	0.06	0.07	0.01	0.03	0.03	0.03	0.01	0.02	0.03
Pr	0.000	0.000	0.01	0.01	0.002	0.002	0.000	0.01	0.01	0.000	0.003	0.01	0.01	0.01	0.01	0.02	0.004	0.02	0.004	0.01	0.01	0.002	0.02
Nd	0.02	0.06	0.01	0.02	0.03	0.04	0.06	0.02	0.02	0.05	0.03	0.08	0.28	0.27	0.13	0.33	0.21	0.34	0.16	0.16	0.12	0.22	0.16
Sm	0.16	0.14	0.12	0.11	0.14	0.14	0.18	0.05	0.14	0.15	0.13	0.67	1.38	2.12	1.38	1.58	0.96	1.44	0.84	1.09	0.85	1.04	1.14
Eu	0.17	0.18	0.08	0.19	0.18	0.15	0.22	0.21	0.18	0.12	0.17	0.06	0.04	0.08	0.06	0.08	0.05	0.05	0.04	0.13	0.04	0.04	0.03
Gd	0.47	0.49	0.55	1.07	1.20	0.95	0.99	1.20	1.15	0.67	0.87	2.12	4.15	5.77	4.02	5.33	3.25	4.33	2.34	4.09	2.54	3.33	2.99
Tb	0.35	0.33	0.33	0.74	0.70	0.69	0.71	0.70	0.76	0.44	0.57	1.07	1.91	2.61	2.02	2.22	1.43	2.13	1.39	2.01	1.22	1.61	1.27
Dy	4.12	3.96	5.40	11.3	11.1	10.8	10.7	10.8	11.8	6.22	8.63	10.3	21.3	26.9	22.8	24.9	16.5	23.3	17.1	22.0	14.5	18.4	15.3
Ho	1.37	1.37	2.11	3.90	3.89	3.91	3.75	3.66	4.24	2.19	3.04	2.89	5.92	7.19	6.12	6.64	4.65	6.34	4.44	6.23	4.25	5.03	4.34
Er	6.28	5.96	10.1	18.4	18.4	17.7	17.3	17.9	20.3	10.5	14.3	12.9	26.4	30.4	26.2	27.3	20.3	28.7	21.5	26.6	19.0	22.4	19.0
Tm	1.70	1.69	2.71	4.77	4.75	4.57	4.02	4.64	5.01	2.66	3.65	3.51	7.02	7.84	7.21	7.49	5.55	7.76	5.80	7.32	5.62	6.14	5.40
Yb	15.0	14.6	25.9	44.8	45.0	43.9	37.6	43.8	47.6	24.9	34.3	38.1	76.3	85.8	80.7	82.0	64.4	86.9	65.2	77.7	59.8	68.6	62.9
Lu	2.71	2.73	4.50	8.00	7.71	7.38	6.23	7.47	8.20	4.21	5.91	6.86	13.4	14.3	14.0	14.6	11.4	15.3	11.4	13.7	11.1	11.9	11.5
Y	7.95	7.81	11.9	23.3	22.9	22.2	21.8	22.8	25.3	13.7	18.0	37.9	73.9	87.4	77.2	81.1	55.0	79.5	58.1	73.4	52.5	59.8	50.5
ΣREE	32.3	31.5	51.9	93.4	93.2	90.3	81.8	90.5	99.4	52.1	71.6	78.6	158	183	165	173	129	177	130	161	119	139	124
δEu	1.94	2.13	0.93	1.67	1.33	1.24	1.56	2.69	1.39	1.15	1.51	0.15	0.05	0.07	0.07	0.09	0.08	0.06	0.08	0.18	0.07	0.07	0.05
Mg	665	666	1110	1110	1030	1060	1100	1110	1080	1160	1010	8.46	8.96	9.44	8.68	10.2	7.29	7.58	9.04	8.98	8.22	8.07	7.34
Sc	17.4	16.3	43.2	83.7	78.7	75.8	56.9	78.9	67.6	30.8	54.9	118	185	234	207	183	179	171	169	159	138	209	200
Ti	63.5	50.0	130	180	280	218	378	158	237	59.1	175	25.3	104	178	108	133	79.3	82.1	93.5	116	79.1	89.5	51.7
Y	7.95	7.81	11.9	23.3	22.9	22.2	21.8	22.8	25.3	13.7	18.0	37.9	73.9	87.4	77.2	81.1	55.0	79.5	58.1	73.4	52.5	59.8	50.5
Zr	13.7	12.4	4.94	23.2	52.8	35.9	25.8	32.0	47.5	2.57	25.1	10.3	29.1	35.9	32.9	34.0	26.2	37.8	25.0	25.9	20.1	27.7	33.2
Hf	0.15	0.14	0.07	0.54	1.03	0.73	0.47	0.65	0.89	0.04	0.47	0.55	1.35	1.67	1.52	1.79	1.15	1.64	1.17	1.28	0.83	1.33	1.76
Nb	20.9	24.5	276	289	216	208	217	215	385	723	257	3150	3810	4370	4080	4280	3490	4240	3240	3440	2810	3550	3840
Mo	1.35	1.33	0.71	0.73	0.77	1.22	0.65	0.49	0.70	0.64	0.86	6.98	8.02	9.70	8.13	7.58	8.02	7.28	9.06	8.36	7.62	8.16	6.96
In	5.02	4.33	0.79	1.37	1.68	1.38	1.47	1.47	1.77	0.68	2.00	12.6	20.3	20.5	20.5	24.0	19.4	22.1	19.2	20.5	17.6	18.3	20.2
Sn	5.87	5.47	5.38	15.5	22.0	18.0	42.5	11.0	21.9	4.99	15.3	36.2	71.5	90.7	71.4	85.8	46.9	87.6	40.4	48.2	33.8	50.7	56.1
Ta	0.22	0.19	3.81	2.37	3.37	2.05	2.55	2.41	4.32	12.8	3.41	123	83.7	114	92.0	122	105	152	97.2	76.2	64.7	86.9	169
U	0.92	0.75	0.59	2.94	5.94	4.39	9.79	1.94	4.97	0.46	3.27	7.28	33.4	58.7	35.8	40.9	18.6	40.0	19.1	29.2	15.4	23.1	17.3
MnO (%)	7.7	7.9	6.8	7.2	6.8	6.9	6.7	6.8	6.6	6.6	7.0	12.9	13.2	12.7	13.1	13.4	13.2	13.3	13.2	13.4	13.1	13.3	12.9
FeO (%)	15.0	14.6	15.7	15.2	15.4	15.6	15.9	15.5	16.1	16.2	15.5	10.4	9.9	10.5	10.4	9.8	10.3	10.4	10.8	10.4	10.4	10.6	10.5
WO_3 (%)	77.0	77.1	77.1	77.1	77.3	77.0	76.9	77.3	76.8	76.6	77.0	76.0	76.0	75.8	75.7	75.7	75.7	75.4	75.2	75.4	75.8	75.3	75.7
FeO/MnO	1.9	1.8	2.3	2.1	2.3	2.3	2.4	2.3	2.4	2.5	2.2	0.8	0.8	0.8	0.8	0.7	0.8	0.8	0.8	0.8	0.8	0.8	0.8

Spots	16PT10a						Xihuashan (16XHS01b-2)															
	13	14	15	16	17	Mean (n = 17)	1	2	3	4	5	6	7	8	9	10	12	13	14	15	16	Mean (n = 15)
La	0.01	0.003	0.02	0.01	0.003	0.007	0.11	0.01	0.04	0.01	0.01	0.01	0.03	0.02	0.01	0.03	0.01	0.003	0.01	0.04	0.01	0.02
Ce	0.04	0.07	0.07	0.03	0.03	0.04	0.47	0.13	0.84	0.22	0.31	0.60	0.57	0.44	0.19	0.54	0.35	0.14	0.35	0.44	0.17	0.38
Pr	0.02	0.03	0.03	0.01	0.01	0.01	0.15	0.07	0.39	0.15	0.22	0.33	0.37	0.23	0.12	0.27	0.22	0.12	0.18	0.30	0.11	0.21
Nd	0.19	0.21	0.35	0.22	0.18	0.21	1.63	0.98	4.91	1.60	2.25	4.28	4.02	3.24	1.24	3.68	2.53	1.67	2.65	3.57	1.82	2.67
Sm	1.22	1.16	1.28	0.85	0.87	1.17	5.24	4.32	15.1	6.40	9.20	15.4	15.0	9.76	5.75	14.7	9.83	7.32	9.31	13.1	6.09	9.76
Eu	0.04	0.03	0.07	0.03	0.03	0.05	0.02	0.01	0.06	0.02	0.02	0.04	0.04	0.04	0.01	0.01	0.02	0.02	0.02	0.02	0.03	0.02
Gd	3.57	4.01	4.21	2.55	2.76	3.61	17.9	17.1	56.0	24.6	37.3	54.8	53.2	39.0	23.0	51.9	35.6	26.2	36.4	47.2	23.4	36.2
Tb	2.06	1.88	2.11	1.35	1.27	1.74	9.70	8.56	26.9	12.9	18.1	26.8	26.7	19.1	11.3	26.4	17.9	12.8	17.7	22.3	12.1	17.9
Dy	22.2	20.0	22.7	15.6	14.8	19.3	113	97.5	335	153	212	313	305	225	132	299	210	142	201	250	138	208
Ho	6.65	5.48	6.24	4.18	3.95	5.33	30.1	26.8	95.2	40.9	59.2	87.7	86.6	64.6	36.4	84.8	56.4	35.6	53.5	66.0	37.7	57.4
Er	29.2	24.4	26.5	18.1	16.9	23.3	117	106	402	167	236	348	344	261	146	346	223	136	214	264	153	231
Tm	8.26	6.96	7.39	5.35	4.85	6.44	24.3	20.8	86.4	33.2	48.6	73.0	72.0	52.6	29.7	73.1	46.3	27.7	44.5	57.0	32.4	48.1

(*continued on next page*)

Table 1 (*continued*)

Spots	16PT10a						Xihuashan (16XHS01b-2)															
	13	14	15	16	17	Mean (n = 17)	1	2	3	4	5	6	7	8	9	10	12	13	14	15	16	Mean (n = 15)
Yb	90.5	75.9	83.3	59.6	52.7	71.2	205	186	790	289	413	659	627	474	256	630	405	220	392	483	286	421
Lu	16.3	13.5	14.5	11.2	9.21	12.6	29.6	26.5	121	42.7	59.4	99.5	93.6	70.7	37.7	96.0	56.6	30.6	57.3	71.2	42.7	62.4
Y	78.4	71.0	80.0	55.2	48.4	65.8	330	301	1278	454	606	988	994	795	446	1020	650	315	668	777	431	670
ΣREE	180	154	169	119	108	145	554	496	1930	771	1100	1680	1630	1220	679	1630	1060	641	1030	1280	733	1100
δEu	0.05	0.05	0.09	0.07	0.07	0.08	0.01	0.00	0.01	0.01	0.003	0.004	0.004	0.01	0.003	0.001	0.004	0.005	0.003	0.003	0.01	0.004
Mg	7.47	7.66	8.23	7.31	7.21	8.24	34.6	35.3	34.1	37.6	36.7	35.6	36.2	34.9	38.4	36.4	34.1	32.9	33.6	63.6	33.2	37.1
Sc	206	214	246	159	183	186	316	312	1500	499	651	1120	1090	886	451	1070	685	370	682	935	461	735
Ti	64.2	61.0	104	96.8	28.6	87.9	19.8	17.0	75.1	18.9	21.8	51.5	49.3	37.0	20.6	47.2	31.5	13.4	27.3	48.6	20.0	33.3
Y	78.4	71.0	80.0	55.2	48.4	65.8	330	301	1280	454	606	988	994	795	446	1020	650	315	668	777	431	670
Zr	62.2	30.8	38.1	19.7	24.2	30.2	14.4	11.2	240	32.5	54.7	164	157	111	25.9	164	74.8	22.4	79.4	157	33.0	89.4
Hf	2.94	1.47	1.93	1.19	1.71	1.49	0.88	0.54	18.2	1.83	3.23	11.3	10.5	8.49	1.62	11.9	5.60	1.59	6.15	13.7	1.99	6.50
Nb	5550	3210	3650	3110	3670	3730	2900	2740	11,000	4280	5750	9170	9220	7580	4180	9160	6810	3750	6840	7730	4070	6340
Mo	7.07	7.74	8.62	9.23	7.52	8.00	111	110	81.1	114	110	102	106	94.9	116	103	89.2	142	72.9	108	52.2	101
In	26.8	21.5	23.2	20.2	17.8	20.3	25.8	25.1	84.4	37.2	48.8	75.1	72.6	61.4	34.4	73.1	48.8	31.6	49.6	63.5	36.4	51.2
Sn	141	57.9	76.3	50.6	48.6	64.3	35.2	24.7	778	74.1	134	507	466	366	52.7	513	192	50.9	224	456	79.2	264
Ta	438	109	93.9	214	204	138	281	163	7900	1160	2150	5910	5760	3710	687	5750	2070	799	2080	5310	1420	3010
U	40.7	19.5	26.5	10.9	9.28	26.2	7.54	3.76	95.0	11.3	19.9	64.1	65.8	46.3	8.54	70.1	30.5	7.01	31.5	53.7	10.3	35.0
MnO(%)	13.5	13.3	13.2	13.6	13.2	13.2	11.1	10.9	10.2	10.5	10.5	10.2	10.5	10.2	10.6	10.4	10.4	10.8	10.2	10.1	10.2	10.4
FeO(%)	10.6	10.6	10.7	10.4	10.6	10.4	11.9	12.1	12.6	12.3	12.2	12.5	12.6	12.5	12.3	12.5	13.0	12.7	12.7	13.5	13.1	12.6
WO_3(%)	74.8	75.3	75.2	75.2	75.3	75.5	76.2	76.1	73.6	75.9	75.7	74.5	74.1	75.0	76.0	74.2	74.8	75.5	75.2	73.6	75.4	75.1
FeO/MnO	0.8	0.8	0.8	0.8	0.8	0.8	1.1	1.1	1.2	1.2	1.2	1.2	1.2	1.2	1.2	1.2	1.3	1.2	1.2	1.3	1.3	1.2

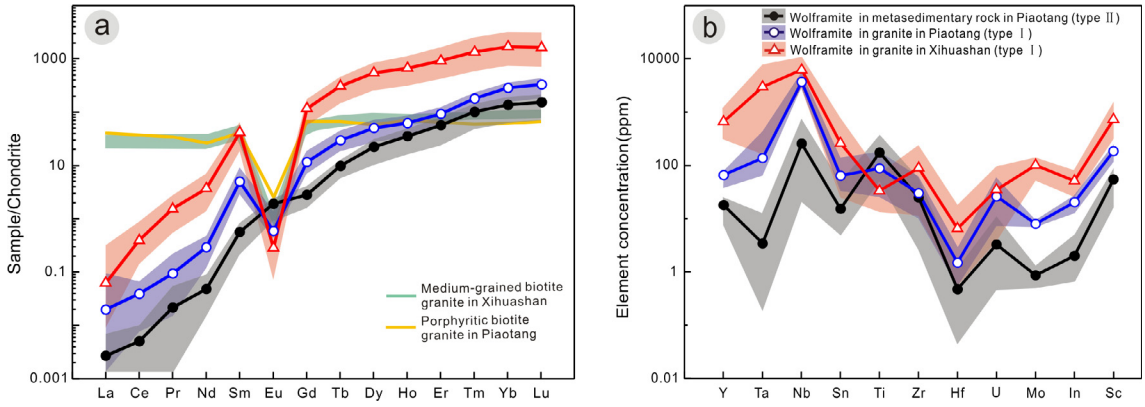

Fig. 9. (a) REE_N patterns of wolframite in the Xihuashan and Piaotang deposits; REE values of chondrite are from Taylor and McLennan (1985); REE contents of the medium-grained biotite granite in Xihuashan and porphyritic biotite granite in Piaotang are from Xiao et al. (2009) and Zhang (2004), respectively. (b) Trace element compositions of wolframite from Xihuashan and Piaotang. The lines with symbols correspond to the average values of LA-ICP-MS analyses per sample and the colored fields represent the values range.

LREE/HREE and Sr values and obviously positive Eu anomalies, differing from the early one. The positive correlation between Sr contents and $^{87}Sr/^{86}Sr$ ratios in scheelite from this type mineralization also reflects that ore formation is closely related to intense fluid metasomatism (Li et al., 2018; Sun and Chen, 2017). The Shimensi veinlet-disseminated scheelite mineralization occurs in intensively altered (especially greisenization) Mesozoic porphyritic biotite granite and Neoproterozoic granodiorite. Greisenization of these granitic rocks transforms plagioclase to mica and quartz, releasing significant amounts of LREE, Eu and Sr into fluids. A source of Ca is critical for scheelite mineralization. Plagioclase in the Mesozoic and Neoproterozoic granitic rocks has average An values of 11.9 and 38.8, respectively (Wang et al. 2015). During greisenization, Ca can be easily released from plagioclase into fluids. Meanwhile, this alteration would consume H^+ and hence increase pH of fluids, which lowers solubility of scheelite in fluids (Wood and Samson, 2000). The alteration of these granitic rocks not only modifies the fluid composition, but also provides necessary Ca to form scheelite (Jiang et al., 2015), and thus is decisive for the formation of veinlet-disseminated scheelite deposits. Therefore, it could be concluded that vein-type wolframite deposits are mainly formed by filling and that veinlet-disseminated scheelite deposits dominantly by metasomatism.

7. Conclusions

(1) In-situ LA-ICP-MS trace element compositions of scheelite and wolframite confirm that the ore-forming fluids for the Shimensi veinlet-disseminated scheelite and the Xihuashan and Piaotang vein-type wolframite deposits are mainly derived from granitic magmas.
(2) The compositional changes of fluids in vein-type deposits are mainly controlled by wolframite crystallization during fluid evolution. In addition to scheelite precipitation, alteration such as greisenization also exerts a significant effect on the composition of fluids in veinlet-disseminated deposits.
(3) Vein-type deposits are mainly formed by filling, whereas veinlet-

Table 2
Trace element analytical results (in ppm) of scheelite by LA-ICP-MS in the Shimensi ore section.

Spots	SM-06	SM-07	SM-09	SM-10	SM-11	SM-12	SM-13	SM-14	SM-15	SM-17	SM-18	SM-20	SM-21	SM-22	SM-23
La	175	96.8	85.2	47.5	115	121	60.6	112	35.8	61.3	57.4	49.8	95.8	123	67.5
Ce	571	292	242	89.5	317	324	116	316	77.1	234	108	212	356	323	290
Pr	82.1	40.9	34.0	9.45	41.9	43.2	11.7	45.0	8.38	41.8	10.6	42.6	57.6	39.3	51.6
Nd	363	184	164	34.8	188	194	40.9	212	33.0	250	33.2	271	289	168	289
Sm	103	57.0	50.9	7.71	50.3	53.4	10.0	57.3	7.76	99.3	6.12	112	85.8	46.5	98.1
Eu	16.2	10.4	8.51	4.46	10.8	11.0	8.25	8.42	2.76	3.51	5.04	12.2	9.40	11.0	8.75
Gd	123	92.1	58.3	9.24	58.5	58.6	10.2	65.8	7.74	146	4.79	154	112	68.8	132
Tb	26.8	19.2	10.2	1.76	11.2	11.1	1.82	11.4	1.26	25.3	0.88	27.6	21.5	14.5	23.2
Dy	193	139	66.4	13.4	80.9	79.2	10.9	77.2	9.12	160	5.18	166	149	112	153
Ho	40.7	31.3	14.2	3.25	18.0	17.6	2.03	16.1	2.13	34.0	1.11	30.3	33.1	25.9	30.8
Er	115	86.1	39.6	10.8	54.0	51.6	5.11	43.6	6.65	87.6	3.13	67.7	87.1	77.8	76.3
Tm	16.9	11.62	5.74	1.90	8.08	7.95	0.79	6.19	1.22	10.9	0.52	7.54	11.2	11.5	8.76
Yb	103	71.4	38.2	15.8	52.1	49.8	5.91	40.8	8.34	59.1	3.70	37.6	60.0	72.5	46.5
Lu	11.4	8.76	4.92	2.40	6.30	6.21	0.80	5.20	1.39	6.70	0.53	3.85	7.36	9.56	5.36
Y	981	746	347	190	429	423	62.1	356	114	885	38.9	317	714	846	601
LREE/HREE	4.85	3.45	5.94	5.86	5.50	5.90	18.2	7.15	8.76	3.57	26.6	4.93	4.82	3.82	5.11
ΣREE	1940	1140	822	252	1010	1030	285	1020	203	1220	241	1200	1370	1100	1280
δEu	0.44	0.44	0.48	1.61	0.61	0.60	2.50	0.42	1.09	0.09	2.84	0.09	0.29	0.59	0.24
Na	493	517	180	64.8	195	198	50.0	183	45.6	291	36.0	179	257	287	205
Sr	57.3	75.8	168	378	57.8	64.7	423	78.9	307	26.9	378	95.1	68.7	53.6	70.1
Nb	n.a.	n.a.	84.6	5.18	114	111	5.08	131	9.15	250	4.07	203	329	166	386
Ta	n.a.	n.a.	3.95	0.09	5.74	5.53	0.12	5.78	0.15	12.8	0.09	4.89	10.2	5.10	12.5
Mo	54.3	38.8	115	54.9	198	192	46.8	125	57.3	127	46.7	33.9	35.9	130	36.9
Pb	n.a.	n.a.	19.9	31.3	15.8	17.2	27.8	16.7	28.8	7.11	31.8	16.9	19.0	16.9	17.0
Th	0.51	4.68	21.9	24.3	0.24	0.25	7.74	0.23	8.97	0.12	12.7	0.14	0.64	0.18	0.12
U	0.24	0.23	5.01	7.19	0.06	0.06	0.51	0.04	1.82	0.03	0.09	0.01	0.12	0.12	0.08

Note: n.a.-not analyzed.

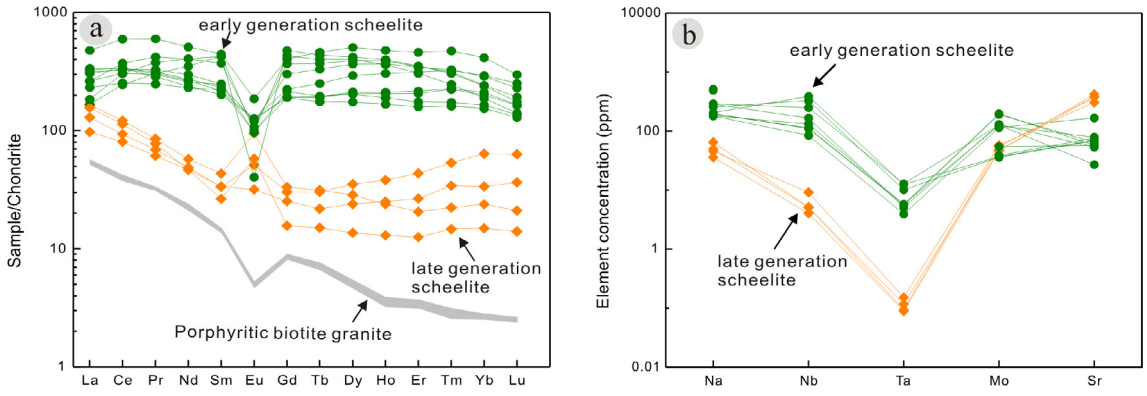

Fig. 10. (a) REE_N patterns of scheelite in the Shimensi ore section; REE values of chondrite and the Mesozoic porphyritic biotite granite in Shimensi are from Taylor and McLennan (1985) and Mao et al. (2015), respectively. (b) Trace element compositions of two generations of scheelite.

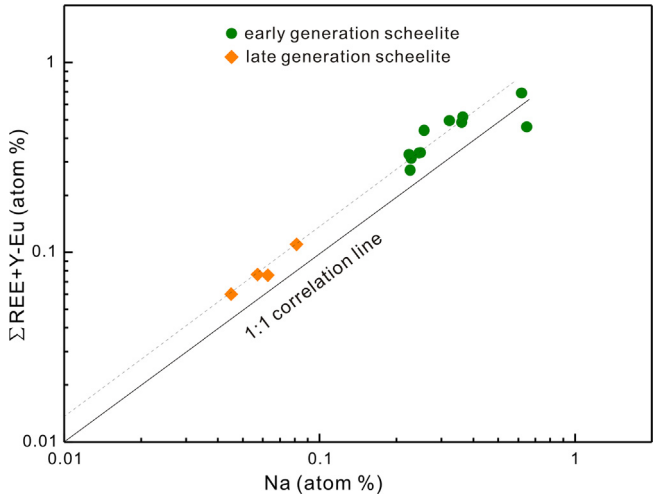

Fig. 11. Plot of Na vs.ΣREE + Y-Eu (in 100 atoms per $CaWO_4$ formula unit) for two generations of scheelite in the Shimensi ore section. The solid line is the 1:1 correlation line assuming no ΣREE + Y-Eu in scheelite with no Na, whereas the dashed line indicates finiteΣREE + Y-Eu contents in scheelite with no Na.

disseminated deposits are associated with metasomatism.

Acknowledgements

This work is financially supported by the National Key R&D Program of China (2016YFC0600207), the National Natural Science Foundation of China (41273053) and the National Key Basic Research Program of China (2012CB416702). We are grateful to Juan Li at School of Earth Sciences and Engineering, Nanjing University for taking CL images. We also thank the staff of the Nanjing FocuMS Technology Co. Ltd. for their kind help in in-situ LA-ICP-MS analysis.

Appendix A. Supplementary data

Supplementary data associated with this article can be found, in the online version, at https://doi.org/10.1016/j.oregeorev.2018.06.004.

References

Arth, J.G., 1976. Behavior of trace elements during magmatic processes: a summary of theoretical models and their applications. J. Res. U.S. Geol. Surv. 4, 41–47.
Brugger, J., Lahaye, Y., Costa, S., Lambert, D., Bateman, R., 2000. Inhomogeneous distribution of REE in scheelite and dynamics of Archaean hydrothermal systems (Mt. Charlotte and Drysdale gold deposits, Western Australia). Contrib. Mineral. Petrol. 139, 251–264.
Bychkov, A.Y., Matveeva, S.S., 2008. Thermodynamic model of the formation of ore bodies at the Akchatau wolframite greisen-vein deposit. Geochem. Int. 46, 867–886.
Chen, J., Lu, J.J., Chen, W.F., Wang, R.C., Ma, D.S., Zhu, J.C., Zhang, W.L., Ji, J.F., 2008. W-Sn-Nb-Ta-bearing granites in the Nanling Range and their relationships to metallogenesis. Geol. J. China Univ. 14, 459–473 (in Chinese with English Abstract).
Chen, J., Wang, R.C., Zhu, J.C., Lu, J.J., Ma, D.S., 2013. Multiple-aged granitoids and related tungsten-tin mineralization in the Nanling Range, South China. Sci. China Earth Sci. 56, 2045–2055.
Codeço, M.S., Weis, P., Trumbull, R.B., Pinto, F., Lecumberri-Sanchez, P., Wilke, F.D.H., 2017. Chemical and boron isotopic composition of hydrothermal tourmaline from the Panasqueira W-Sn-Cu deposit, Portugal. Chem. Geol. 468, 1–16.
Crowe, D.E., Riciputi, L.R., Bezenek, S., Ignatiev, A., 2001. Oxygen isotope and trace element zoning in hydrothermal garnets: Windows into large-scale fluid-flow behavior. Geology 29, 479–482.
Dewaele, S., Clercq, F.D., Hulsbosch, N., Piessens, K., Boyce, A., Burgess, R., Muchez, P., 2016. Genesis of the vein-type tungsten mineralization at Nyakabingo (Rwanda) in the Karagwe-Ankole belt, Central Africa. Miner. Deposita 51, 283–307.
Ghaderi, M., Palin, J.M., Campbell, I.H., Sylvester, P.J., 1999. Rare earth element systematics in scheelite from hydrothermal gold deposits in the Kalgoorlie-Norseman region, Western Australia. Econ. Geol. 94, 423–437.
Giuliani, G., Li, Y.D., Sheng, T.F., 1988. Fluid inclusion study of Xihuashan tungsten deposit in the southern Jiangxi province, China. Miner. Deposita 23, 24–33.
Goldmann, S., Melcher, F., Gäbler, H.E., Dewaele, S., Clercq, F.D., Muchez, P., 2013. Mineralogy and trace element chemistry of ferberite/reinite from tungsten deposits in Central Rwanda. Minerals 3, 121–144.
Gu, J.Y., 1979. A significant indicator of mineralized veinlet (zone) for finding blind deposits. Geol. Rev. 25, 47–52 (in Chinese).
Gu, J.Y., 1984. The surface indicator zones of the blind-semi-blind tungsten vein deposits in South China. Min. Deposita 3, 67–76 (in Chinese with English Abstract).
Guo, C.L., Chen, Y.C., Zeng, Z.L., Lou, F.S., 2012. Petrogenesis of the Xihuashan granites in southeastern China: Constraints from geochemistry and in-situ analyses of zircon U-Pb-Hf-O isotopes. Lithos 148, 209–227.
Guo, Z.J., Li, J.W., Xu, X.Y., Song, Z.Y., Dong, X.Z., Tian, J., Yang, Y.C., She, H.Q., Xiang, A.P., Kang, Y.J., 2016. Sm-Nd dating and REE composition of scheelite for the Honghuaerji scheelite deposit, Inner Mongolia, Northeast China. Lithos 261, 307–321.
Harlaux, M., Mercadier, J., Marignac, C., Peiffert, C., Cloquet, C., Cuney, M., 2018. Tracing metal sources in peribatholitic hydrothermal W deposits based on the chemical composition of wolframite: The example of the Variscan French Massif Central. Chem. Geol. 479, 58–85.
He, Z.Y., Xu, X.S., Zou, H.B., Wang, X.D., Yu, Y., 2010. Geochronology, petrogenesis and metallogeny of Piaotang granitoids in the tungsten deposit region of South China. Geochem. J. 44, 299–313.
Heinrich, C.A., 1990. The chemistry of hydrothermal tin(-tungsten) ore deposition. Econ. Geol. 85, 457–481.
Higgins, N.C., 1985. Wolframite deposition in a hydrothermal vein system: the Gray River tungsten prospect, Newfoundland, Canada. Econ. Geol. 80, 1297–1327.
Hu, R.Z., Wei, W.F., Bi, X.W., Peng, J.T., Qi, Y.Q., Wu, L.Y., Chen, Y.W., 2012. Molybdenite Re-Os and muscovite $^{40}Ar/^{39}Ar$ dating of the Xihuashan tungsten deposit, central Nanling district, South China. Lithos 150, 111–118.
Huang, L.C., Jiang, S.Y., 2014. Highly fractionated S-type granites from the giant Dahutang tungsten deposit in Jiangnan Orogen, Southeast China: geochronology, petrogenesis and their relationship with W-mineralization. Lithos 202–203, 207–226.
Huang, X.W., Gao, J.F., Qi, L., Zhou, M.F., 2015. In-situ LA-ICP-MS trace elemental analyses of magnetite and Re-Os dating of pyrite: The Tianhu hydrothermally remobilized sedimentary Fe deposit, NW, China. Ore Geol. Rev. 65, 900–916.
Jiang, S.Y., Peng, N.J., Huang, L.C., Xu, Y.M., Zhan, G.L., Dan, X.H., 2015. Geological characteristics and ore genesis of the giant tungsten deposits from the Dahutang ore-concentrated district in northern Jiangxi Province. Acta Petrol. Sin. 31, 639–655 (in Chinese with English Abstract).
Korges, M., Weis, P., Lüders, V., Laurent, O., 2018. Depressurization and boiling of a single magmatic fluid as a mechanism for tin-tungsten deposit formation. Geology 46, 75–78.
Lecumberri-Sanchez, P., Vieira, R., Heinrich, C.A., Pinto, F., Wälle, M., 2017. Fluid-rock interaction is decisive for the formation of tungsten deposits. Geology 45, 579–582.

Li, C., Zhou, L.M., Zhao, Z., Zhang, Z.Y., Zhao, H., Li, X.W., Qu, W.J., 2018. In-situ Sr isotopic measurement of scheelite using fs-LA-MC-ICPMS. J. Asian Earth Sci. 160, 38–47.
Li, G.L., Hua, R.M., Hu, D.Q., Huang, X.E., Zhang, W.L., Wang, X.D., 2010. Petrogenesis of Shilei quartz diorite in southern Jiangxi: Constraints from petrochemistry, trace elements of accessory minerals, zircon U-Pb dating ad Sr-Nd-Hf isotopes. Acta Petrol. Sin. 26, 903–918 (in Chinese with English Abstract).
Li, H.Q., Liu, J.Q., Wei, L., 1993. The Study on Fluid Inclusion Geochronology of Hydrothermal Deposits and Its Application. Geological Publishing House, Beijing, pp. 1–126 (in Chinese).
Li, Y.D., Sheng, J.F., Bel, L.L., Giuliani, G., 1986. Evidence for the lower continental crustal origin of the Xihuashan granite. Acta Geol. Sin. 60, 47–64.
Li, X.H., Li, W.X., Li, Z.X., Lo, C.H., Wang, J., Ye, M.F., Yang, Y.H., 2009. Amalgamation between the Yangtze and Cathaysia Blocks in South China: Constraints from SHRIMP U-Pb zircon ages, geochemistry and Nd-Hf isotopes of the Shuangxiwu volcanic rocks. Precambrian Res. 174, 117–128.
Liu, J.Q., 1989. The Xihuashan granite and its mineralization. Bull. Chin. Acad. Geol. Sci. 19, 83–105 (in Chinese with English Abstract).
Liu, Y.J., Cao, L.M., 1987. Introduction to Elemental Geochemistry. Geological Publishing House, Beijing, pp. 98–112 (in Chinese).
Liu, Y.S., Hu, Z.C., Gao, S., Günther, D., Xu, J., Gao, C.G., Chen, H.H., 2008. *In situ* analysis of major and trace elements of anhydrous minerals by LA-ICP-MS without applying an internal standard. Chem. Geol. 257, 34–43.
Lv, K., Wang, Y., Xiao, J., 2011. Geochemistry characteristics of Xihuashan granite and structural environment discussion. J. East China Inst. Technol. 34, 117–128 (in Chinese with English Abstract).
Mao, J.W., Cheng, Y.B., Chen, M.H., Franco, P., 2013a. Major types and time-space distribution of Mesozoic ore deposits in South China and their geodynamic settings. Miner. Deposita 48, 267–294.
Mao, J.W., Xie, G.Q., Guo, C.L., Chen, Y.C., 2007. Large-scale tungsten-tin mineralization in the Nanling region, South China: Metallogenic ages and corresponding geodynamic processes. Acta Petrol. Sin. 23, 2329–2338 (in Chinese with English Abstract).
Mao, Z.H., Cheng, Y.B., Liu, J.J., Yuan, S.D., Wu, S.H., Xiang, X.K., Luo, X.H., 2013b. Geology and molybdenite Re-Os age of the Dahutang granite-related veinlets-disseminated tungsten ore field in the Jiangxi Province, China. Ore Geol. Rev. 53, 422–433.
Mao, Z.H., Liu, J.J., Mao, J.W., Deng, J., Zhang, F., Meng, X.Y., Xiong, B.K., Xiang, X.K., Luo, X.H., 2015. Geochronology and geochemistry of granitoids related to the giant Dahutang tungsten deposit, middle Yangtze River region, China: Implications for petrogenesis, geodynamic setting, and mineralization. Gondwana Res. 28, 816–836.
Mu, Z.G., Huang, F.S., Chen, C.Y., Zheng, S.H., Fan, S.L., Liu, D.R., Mei, Y.W., 1982. Oxygen, hydrogen and carbon isotope studies of Piaotang and Xihuashan quartz vein-type tungsten deposits, Jiangxi Province. In: Hepworth, J.V., Zhang, Y.H. (Eds.), Proceedings of Symposium on Tungsten Geology. Indonesia, Bandung, ESCAP/RMRDC and Geological Publishing House, Beijing, pp. 385–401.
No. 2 Team of Jiangxi Metallurgical Geology, 1978. Compilation for Tungsten Deposits in South Jiangxi Province, China, pp. 1–205 (in Chinese).
No. 916 Geological Team, Jiangxi Bureau of Geology, Mineral Resources, Exploration and Development, 2012. The Exploration Report of the Shimensi, North Portion of the Dahutang Tungsten Deposit, Wuning County, Jiangxi Province. Jiangxi Jutong Mining Corporation, pp. 1–224 (in Chinese).
O'Reilly, C., Gallagher, V., Feely, M., 1997. Fluid inclusion study of the Ballinglen W-Sn-sulphide mineralization, SE Ireland. Miner. Deposita 32, 569–580.
Reich, M., Deditius, A., Chryssoulis, S., Li, J.W., Ma, C.Q., Parada, M.A., Barra, F., Mittermayr, F., 2013. Pyrite as a record of hydrothermal fluid evolution in a porphyry copper system: A SIMS/EMPA trace element study. Geochim. Cosmochim. Acta 104, 42–62.
Shan, F., 1976. The geological characteristics of tungsten-tin deposits of a quartz veinlets-zone type. Acta Geol. Sin. 1, 1–16 (in Chinese with English Abstract).
Shannon, R.D., 1976. Revised effective ionic radii and systematic studies of interatomic distances in halides and chalcogenides. Acta Crystallogr. 32, 751–767.
Sheng, J.F., Liu, L.J., Wang, D.H., Chen, Z.H., Ying, L.J., Huang, F., Wang, J.H., Zeng, L., 2015. A preliminary review of metallogenic regularity of tungsten deposits in China. Acta Geol. Sin. (Engl. Ed.) 89, 1359–1374.
Shu, L.S., Zhou, X.M., Deng, P., Yu, X.Q., 2006. Principal geological features of Nanling tectonic belt, South China. Geol. Rev. 52, 251–265 (in Chinese with English Abstract).
Song, G.X., Qin, K.Z., Li, G.M., Evans, N.J., Chen, L., 2014. Scheelite elemental and isotopic signatures: Implications for the genesis of skarn-type W-Mo deposits in the Chizhou Area, Anhui Province, Eastern China. Am. Mineral. 99, 303–317.
Štemprok, M., Pivec, E., Langrová, A., 2005. The petrogenesis of a wolframite-bearing greisen in the Vykmanov granite stock, Western Krušné hory pluton (Czech Republic). Bull. Geosci. 80, 163–184.
Sun, K.K., Chen, B., 2017. Trace elements and Sr-Nd isotopes of scheelite: Implications for the W-Cu-Mo polymetallic mineralization of the Shimensi deposit, South China. Am. Mineral. 102, 1114–1128.
Sushchevskaya, T.M., Bychkov, A.J., 2009. Thermodynamic modeling of cassiterite-wolframite ore formation at the Iultin Sn-W deposit. Geochim. Cosmochim. Acta 73, 131–159.
Taylor, S.R., McLennan, S.M., 1985. The Continental Crust: Its Composition and Evolution. Blackwell Scientific Publications, Oxford, pp. 1–312.
Vallance, J., Cathelineau, M., Marignac, C., Boiron, M.C., Fourcade, S., Martineau, F., Fabre, C., 2001. Microfracturing and fluid mixing in granites: W-(Sn) ore deposition at Vaulry (NW French Massif Central). Tectonophysics 336, 43–61.
Wang, H., Feng, C.Y., Li, D.X., Xiang, X.K., Zhou, J.H., 2015. Sources of granitoids and ore-forming materials of Dahutang tungsten deposit in northern Jiangxi Province: Constraints from mineralogy and isotopic tracing. Acta Petrol. Sin. 31, 725–739 (in Chinese with English Abstract).
Wang, R.C., Fontan, F., Chen, X.M., Hu, H., Liu, C.S., Xu, S.J., de Parseval, P., 2003. Accessory minerals in the Xihuashan Y-enriched granitic complex, southern China: A record of magmatic and hydrothermal stages of evolution. Can. Mineral. 41, 727–748.
Wang, X.L., Zhou, J.C., Griffin, W.L., Wang, R.C., Qiu, J.S., O'reilly, S.Y., Xu, X.S., Liu, X.M., Zhang, G.L., 2007. Detrital zircon geochronology of Precambrian basement sequences in the Jiangnan orogen: Dating the assembly of the Yangtze and Cathaysia Blocks. Precambrian Res. 159, 117–131.
Wang, X.L., Zhou, J.C., Griffin, W.L., Zhao, G.C., Yu, J.H., Qiu, J.S., Zhang, Y.J., Xing, G.F., 2014. Geochemical zonation across a Neoproterozoic orogenic belt: Isotopic evidence from granitoids and metasedimentary rocks of the Jiangnan orogen, China. Precambrian Res. 242, 154–171.
Wang, Z.H., Zhou, Y.Z., 1982. Two-layer mineralization characteristics and genetic model of the Xihuashan deposit. In: Hepworth, J.V., Zhang, Y.H. (Eds.), Proceedings of Symposium on Tungsten Geology. Indonesia, Bandung, ESCAP/RMRDC and Geological Publishing House, Beijing, pp. 197–205.
Wei, W.F., Hu, R.Z., Bi, X.W., Peng, J.T., Su, W.C., Song, S.Q., Shi, S.H., 2012. Infrared microthermometric and stable isotopic study of fluid inclusions in wolframite at the Xihuashan tungsten deposit, Jiangxi province, China. Miner. Deposita 47, 589–605.
Wood, S.A., Samson, I.M., 2000. The hydrothermal geochemistry of tungsten in granitoid environments: I. Relative solubilities of ferberite and scheelite as a function of T, P, pH, and m_{NaCl}. Econ. Geol. 95, 143–182.
Xiang, X.K., Liu, X.M., Zhan, G.N., 2012. Discovery of Shimensi super-large tungsten deposit and its prospecting significance in Dahutang area, Jiangxi Province. Resour. Surv. Environ. 33, 141–151 (in Chinese with English Abstract).
Xiang, X.K., Wang, P., Zhan, G.N., Sun, D.M., Zhong, B., Qian, Z.Y., Tan, R., 2013. Geological characteristics of Shimensi tungsten polymetallic deposit in northern Jiangxi Province. Mineral Deposits 32, 1171–1187 (in Chinese with English Abstract).
Xiao, J., Wang, Y., Hong, Y.L., Zhou, Y.Z., Xie, M.H., Wang, D.S., Guo, J.S., 2009. Geochemistry characteristics of Xihuashan tungsten granite and its relationship to tungsten metallogenesis. J. East China Inst. Technol. 32, 22–31 (in Chinese with English Abstract).
Xiong, Y.Q., Shao, Y.J., Zhou, H.D., Wu, Q.H., Liu, J.P., Wei, H.T., Zhao, R.C., Cao, J.Y., 2017. Ore-forming mechanism of quartz-vein-type W-Sn deposits of the Xitian district in SE China: Implications from the trace element analysis of wolframite and investigation of fluid inclusions. Ore Geol. Rev. 83, 152–173.
Zhang, L.G., 1988. Oxygen isotope studies of wolframite in tungsten ore deposits of South China. Chin. J. Geochem. 7, 109–119.
Zhang, R.Q., Lu, J.J., Lehmann, B., Li, C.Y., Li, G.L., Zhang, L.P., Guo, J., Sun, W.D., 2017. Combined zircon and cassiterite U-Pb dating of the Piaotang granite-related tungsten-tin deposit, southern Jiangxi tungsten district, China. Ore Geol. Rev. 82, 268–284.
Zhang, S.M., 2012. In: Mineralogy and Deposit Characteristics on the Dajishan Tungsten Deposit in Jiangxi Province. China University of Geosciences, Beijing, China, pp. 1–60 (in Chinese with English Abstract).
Zhang, W.L., 2004. The study on the characteristics and metallogenesis of granites in Dajishan and Piaotang tungsten deposits, southern Jiangxi Province (unpublished doctoral thesis). Nanjing University, Nanjing, China, pp. 1–160 (in Chinese with English Abstract).
Zhang, Y.X., Liu, Y.M., Gao, S.D., He, Q.G., 1990. REE geochemical characteristics of tungsten minerals as a discriminant indicator of genetic types of ore deposits. Chin. J. Geochem. 9, 319–329.
Zhao, W.W., Zhou, M.F., 2015. In-situ LA-ICP-MS trace elemental analyses of magnetite: The Mesozoic Tengtie skarn Fe deposit in the Nanling Range, South China. Ore Geol. Rev. 65, 872–883.
Zhao, W.W., Zhou, M.F., Li, Y.H.M., Zhao, Z., Gao, J.F., 2017. Genetic types, mineralization styles, and geodynamic settings of Mesozoic tungsten deposits in South China. J. Asian Earth Sci. 137, 109–140.
Zhao, W.W., Zhou, M.F., Williams-Jones, A.E., Zhao, Z., 2018. Constraints on the uptake of REE by scheelite in the Baoshan tungsten skarn deposit, South China. Chem. Geol. 477, 123–136.
Zhou, X.M., Sun, T., Shen, W.Z., Shu, L.S., Niu, Y.L., 2006. Petrogenesis of Mesozoic granitoids and volcanic rocks in South China: A response to tectonic evolution. Episodes 29, 26–33.
Zhu, Y.N., Peng, J.T., Liu, S.Y., Sun, Y.Z., 2014. Mineral deposit geology and trace element geochemistry of wolframite from the Woxi deposit, western Hunan, China. Geochimica 43, 287–300 (in Chinese with English Abstract).
Zhu, Z.Y., Wang, R.C., Che, X.D., Zhu, J.C., Wei, X.L., Huang, X.E., 2015. Magmatic-hydrothermal rare-element mineralization in the Songshugang granite (northeastern Jiangxi, China): Insights from an electron-microprobe study of Nb-Ta-Zr minerals. Ore Geol. Rev. 65, 749–760.